Primary motor cortex drives expressive facial movements related to reward processing in mice

Wanru Li[1,2,3]†, Takashi Nakano[4,5,6]†, Kohta Mizutani[2,7], Masahiro Kawatani[1,2,3], Takanori Matsubara[1,2], Teruko Danjo[1], Yasutaka Mukai[2], Akihiro Yamanaka[2], Hikaru Ito[8,9], Hidenori Aizawa[8], Carl C. H. Petersen[10], Junichiro Yoshimoto[5,6,11]*, Takayuki Yamashita[1,2,6]*

Short title: Cortical drive of expressive facial movements

[1] Department of Physiology, Fujita Health University School of Medicine, Toyoake, Japan.
[2] Department of Neuroscience II, Research Institute of Environmental Medicine, Nagoya University, Nagoya, Japan.
[3] Department of Functional Anatomy & Neuroscience, Graduate School of Medicine, Nagoya University, Nagoya, Japan.
[4] Department of Computational Biology, Fujita Health University School of Medicine, Toyoake, Japan.
[5] Nara Institute of Science and Technology, Ikoma, Japan.
[6] International Center for Brain Science (ICBS), Fujita Health University, Toyoake, Japan.
[7] Laboratory for Advanced Brain Functions, Institute for Protein Research, Osaka University, Osaka, Japan.
[8] Department of Neurobiology, Graduate School of Biomedical and Health Sciences, Hiroshima University, Hiroshima, Japan.
[9] Research Facility Center for Science and Technology, Kagawa University, Kagawa, Japan.
[10] Laboratory of Sensory Processing, Brain Mind Institute, Faculty of Life Sciences, École Polytechnique Fédérale de Lausanne (EPFL), Lausanne, Switzerland.
[11] Department of Biomedical Data Science, Fujita Health University School of Medicine, Toyoake, Japan.

† These authors contributed equally to this work.

* Correspondence: takayuki.yamashita@fujita-hu.ac.jp and juniti-y@is.naist.jp

ABSTRACT

Animals exhibit expressive facial movements in a wide range of behavioral contexts. However, the underlying neural mechanisms remain enigmatic. In reward-based learning tasks, mice make expressive movements with their whiskers and nose at the timings of reward expectation and acquisition. Here we show that optogenetic stimulation of midbrain dopamine neurons (oDAS) as a reward is sufficient to induce such expressive movements. Pavlovian conditioning with a sensory cue and oDAS elicited both cue-locked (reward-expecting) and oDAS-aligned (reward-acquiring) orofacial movements. Inhibition or knock-out of dopamine D1 receptors in the nucleus accumbens inhibited oDAS-induced motion but spared cue-locked motion. Silencing the whisker primary motor cortex (wM1) abolished both oDAS-induced and cue-locked orofacial movements. We found specific neuronal populations in wM1 representing either oDAS-aligned or cue-locked whisker movements. Thus, reward-acquiring and reward-expecting facial movements are driven by accumbal D1 receptor-dependent and -independent neuronal mechanisms, respectively, both dominantly regulated by wM1 activity.

INTRODUCTION

Classical observations suggest that various animals exhibit facial and other expressive movements (*1*–*4*). More recent studies revealed that facial expressions in rodents carry multi-dimensional information about their emotional states, including pleasure and disgust (*5*–*8*). Making facial expressions must involve coordinated activities of the facial musculature. However, the neural mechanisms underlying the control of expressive facial movements in different behavioral contexts remain poorly understood.

In reward-based tasks, mice exhibit expressive orofacial movements which are not instructed or necessary for task execution (*9*–*13*). For example, mice well-trained for a stimulus-reward association task often show whisker movements immediately after reward-predicting cue presentation (*9*, *10*, *13*), which may constitute a facial expression of reward expectation (*11*, *14*). Acquisition of liquid reward by licking also seems to induce whisker and other facial movements (*8*, *10*, *11*, *13*). However, licking behavior is phase-locked to breathing, sniffing, and other orofacial activities (*15*–*17*), making it challenging to disentangle expressive facial movements elicited purely by reward-related internal states in these liquid reward-based tasks. In addition, little is known about which neuronal populations are directly involved in forming such expressive facial movements.

Dopamine (DA) neurons in the ventral tegmental area (VTA) play a central role in mediating motivated behaviors and are supposed to form part of the reward circuit of the brain (*18*–*20*). Transient stimulation of VTA-DA neurons is reinforcing (*21*–*23*) and can replace some aspects of liquid reward (*24*). The VTA-DA neurons in mice fire phasically upon reward expectation and acquisition (*25*–*27*), the timings similar to expressive whisker movements in reward-based tasks (*9*, *10*, *13*). Therefore, the VTA-DA neurons may be involved in making expressive facial movements during reward-based tasks.

The primary motor cortex (M1) is another candidate for a brain region that may be involved in expressive orofacial movements. There has been compelling evidence that stimulation of specific areas within the orofacial M1 of rodents triggers movements in the whisker and nose (*28*–*32*). Neurons in the orofacial M1 encode various aspects of movements in the whisker and nose (*31*–*35*). Nevertheless, it is unknown whether the orofacial M1 plays a causal role in constituting expressive facial movements that reflect any internal or emotional states. Instead, stimulation of the insular cortex is reported to elicit facial

expressions of tastants-evoked (*8*, *36*) and other (*36*) emotional states. On the other hand, tastants-evoked orofacial expressions in rats remain intact even after chronic decerebration (*37*, *38*).

In this study, we confirmed that stereotypical whisker movements were induced at the timings of reward expectation and acquisition in stimulus-water reward association tasks. Using optogenetic stimulation of VTA-DA neurons (oDAS) as a reward, we show that such reward-related orofacial movements could be elicited in the absence of goal-directed action. Further perturbational analyses revealed that the mesolimbic DA pathway is involved in expressive orofacial movements upon reward acquisition but not in those upon reward expectation. However, silencing the whisker M1 (wM1) blocked orofacial movements upon both reward expectation and reward acquisition. We found that specific subpopulations in the wM1 represent expressive orofacial movements upon reward expectation and acquisition. Our results thus suggest that wM1 dominantly regulates expressive orofacial movements related to reward processing.

RESULTS

Whisker movements during reward-based learning tasks

When mice learn a simple stimulus-reward association task, some orofacial movements become aligned to task events (*10*). We first analyzed the whisker movement data in our previous recordings using mice performing a whisker detection task, in which thirsty mice learned to lick for water reward in response to a whisker deflection (*39*; Fig. 1A). Expert mice well-trained for the task exhibited a rapid whisker protraction immediately after the reward-associated, brief (1 ms) whisker stimulation in hit trials (Fig. 1B), which had a significantly larger amplitude compared to miss trials (hit 15.8 ± 2.2 deg, miss 5.6 ± 1.0 deg, n = 6 mice,

p = 0.013; Fig. 1C). Such a rapid cue-locked whisker protraction in hit trials was absent in novice mice with low task proficiency (Fig. 1B). The cue-locked whisker protraction started before the onset of goal-directed licking (the latency of whisker protraction 51.7 ± 15.2 ms, the onset latency of licking 213.3 ± 19.2 ms, n = 6 mice, p = 0.0059). Therefore, the cue-locked whisker protraction might be related to the internal states of reward expectation. These expert mice also showed active whisker movements after reward acquisition in hit trials, some of which appeared similar to exploratory whisking (Fig. 1B; *29*, *30*). Total whisker movements (ΣWM) during 1 s after the reward time window were larger in hit trials than in miss trials (hit 381 ± 59 deg, miss 156 ± 31 deg, n = 6 mice, p = 0.0052, Bonferroni's multiple comparison test; Fig. 1C). In contrast to the learning-dependent nature of the cue-locked whisker movements, task learning did not change the ΣWM after hits (novice hit 444 ± 96 deg, n = 6 mice, p = 0.93, Bonferroni's multiple comparison test vs. expert hit; Fig. 1C). Thus, stereotypical whisker movements could be observed at the timings of reward expectation and a second after reward acquisition during a whisker-detection task.

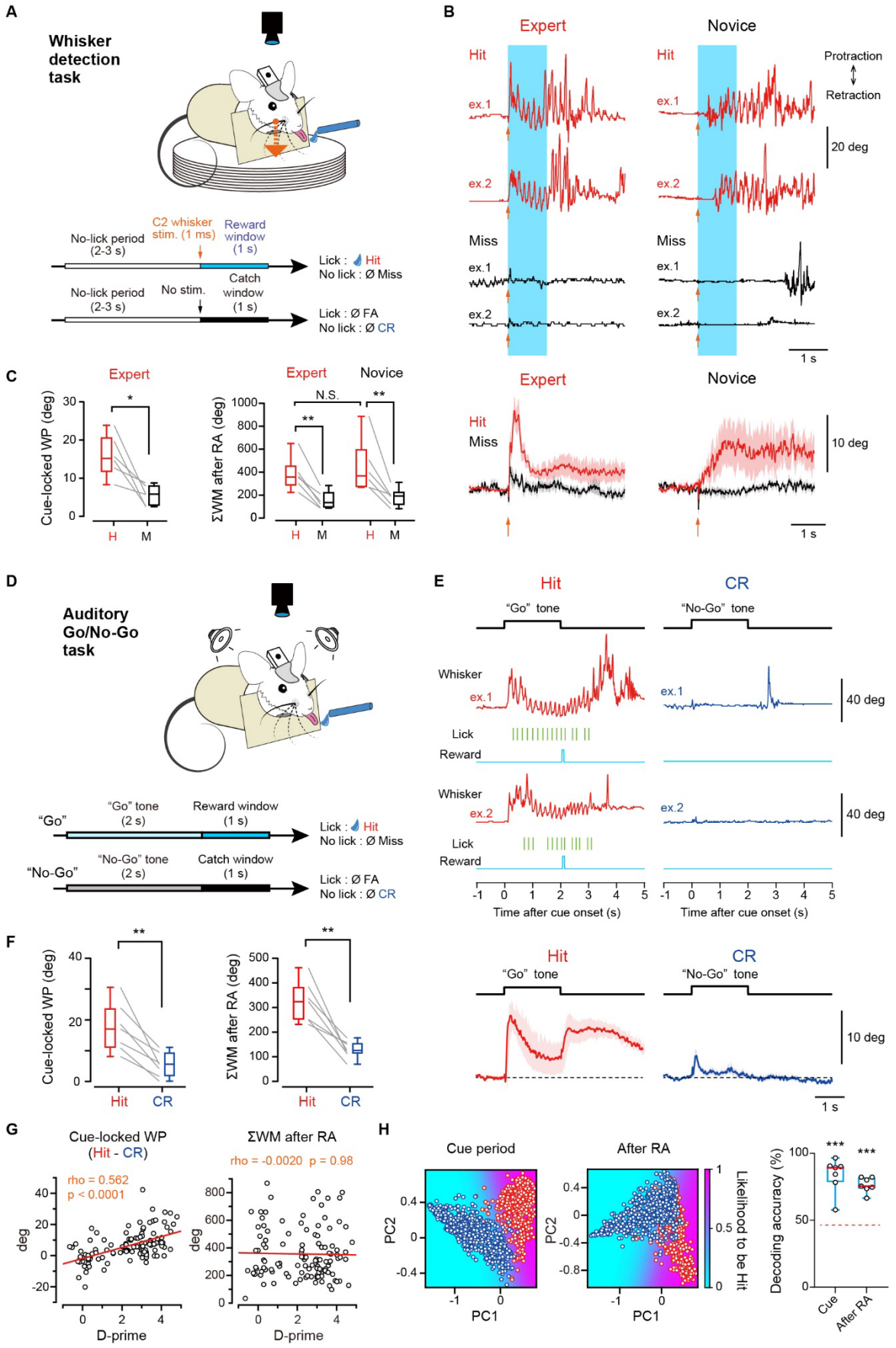
A
Whisker detection task
No-lick period (2-3 s)
C2 whisker stim. (1 ms)
Reward window (1 s)
Lick : Hit
No lick : Ø Miss
No-lick period (2-3 s)
No stim.
Catch window (1 s)
Lick : Ø FA
No lick : Ø CR
B
Expert
Novice
Hit
ex.1
ex.2
Miss
Protraction
Retraction
20 deg
1 s
10 deg
C
Cue-locked WP (deg)
ΣWM after RA (deg)
N.S.
H
M
D
Auditory Go/No-Go task
"Go"
"Go" tone (2 s)
Reward window (1 s)
"No-Go"
"No-Go" tone (2 s)
Catch window (1 s)
E
CR
Whisker
Lick
Reward
40 deg
Time after cue onset (s)
F
Hit
CR
G
Cue-locked WP (Hit - CR)
rho = 0.562
p < 0.0001
ΣWM after RA
rho = -0.0020 p = 0.98
deg
D-prime
H
Cue period
After RA
PC1
PC2
Likelihood to be Hit
Decoding accuracy (%)
Cue
After RA

Fig. 1. Stereotypical whisker movements of mice performing stimulus-reward association tasks. (**A**) Schematic for the whisker detection task. FA: false alarm, CR: correct rejection. (**B**) Top, example traces of the whisker position in hit (red) and miss (black) trials during the whisker detection task, obtained from an expert (left) and novice (right) mouse. An arrow indicates the timing of whisker stimulation. Light blue shadows indicate the reward time window. Bottom, grand average traces of the whisker position (n = 6 mice for each). Shadows of grand average traces: ± SEM. (**C**) Amplitudes of the cue-locked whisker protraction (WP) (left) and the total whisker movements (ΣWM) 0–1s after reward time window (right), in hit (H) and miss (M) trials during the whisker detection task. RA: reward acquisition. *p < 0.05, ** p < 0.01, N.S., not significant, paired *t* test (cue-locked WP) and Bonferroni's multiple comparison test (ΣWM after RA). (**D**) Schematic for the auditory Go/No-Go task. (**E**) Top, example traces of the whisker position in hit (red) and CR (blue) trials during the auditory Go/No-Go task, obtained from a well-trained expert mouse. The timings of the sound cue presentation (black), licking (green), and the reward presentation (light blue) are also shown. Bottom, grand average traces of the whisker position in hit (red) and CR (blue) trials, obtained from expert mice (n = 7 mice for each). (**F**) The cue-locked WP amplitude (left) and ΣWM 0–1s after the reward time window (right) during the auditory Go/No-Go task. **p < 0.01, paired *t* test. (**G**) The difference in the cue-locked WP amplitude between hit and CR trials was positively correlated with task proficiency (d-prime) (left), whereas the ΣWM 0–1s after the reward time window of hit trials was not correlated with task performance (right). Open circles represent individual data of each experimental day, obtained from 10 mice. The regression line (red, solid line) is superimposed. (**H**) Example principal component (PC) analyses of whisker time plots from an expert mouse during the cue period (left) and 0–1 s after reward time window (after RA, middle) of hit (red) and CR (blue) trials (see Materials and Methods). Decoding accuracy by the model (right) was significantly higher than the chance level for both cue period and after RA (n = 7 mice). The solid red line in the box plots indicates the median. The dashed red line indicates the mean chance level. ***p < 0.001, Dunnett's multiple comparison test vs. the chance level. Thin lines (C and F) and open circles (H) indicate individual data.

We next examined whether the task-aligned whisker movements seen in the whisker detection task are specific for a task involving whisker sensation. We trained mice for an auditory Go/No-Go task where whisker sensation or motion is not required for task execution. We set the reward time window (1 s) after a 2-s auditory cue presentation (Fig. 1D) to well separate the timings of expectation and acquisition of water reward. Expert mice for the

auditory task exhibited a rapid cue-locked whisker protraction (17.4 ± 5.5 deg, n = 7 mice) and active whisker movements after reward acquisition (ΣWM 0–1 s after the reward window, 320 ± 32 deg, n = 7 mice) in hit trials, both of which were more prominent than in correct rejection (CR) trials (Fig. 1, E and F). In the auditory task, both Go and No-Go sound cues equally elicited a rapid whisker protraction in novice mice (fig S1, A and B), which might be a reflex motor action to a salient auditory stimulus. However, the difference in the amplitude of the cue-locked whisker protraction between hits and CR trials became more prominent as the mice learned the task (Fig. 1G). In contrast, task learning did not change ΣWM after hits (Fig. 1G). These results are essentially the same as those in the whisker detection task. Our machine-learning models, which were only based on the whisker time plots obtained from expert mice during the cue period or 0–1 s after the reward time window, accurately discriminated hit trials over CR trials (decoding accuracy, cue period 83.8 ± 4.8 %, after reward window 76.4 ± 2.1 %, n = 7 mice, Fig. 1H), suggesting that whisker movements with distinct properties are elicited upon reward expectation and after reward acquisition. Thus, stereotypical whisker movements at the timings of reward expectation and a second after reward acquisition are observed generally in stimulus-reward association tasks.

Orofacial movements evoked by oDAS

The stereotypical whisker movements seen in our reward-based tasks (Fig. 1) may be a part of expressive facial movements reflecting expectation and acquisition of a reward (*8*, *11*, *14*). However, motor actions for acquiring liquid reward (i.e., licking) have a specific pattern frequency (5–8 Hz) and are phase-locked to whisker movements (fig S1, C to F) and many other orofacial movements (*15*–*17*), which could add or reduce dimensions of expressive facial movements. Therefore, we next built an experimental setting to reward mice without

inducing any motor actions required for task execution. We implanted an optic fiber unilaterally over the VTA of transgenic mice expressing channelrhodopsin 2 (ChR2) in DA neurons (DAT-ChR2, Fig. 2A). We first tested whether a brief (1 s) train of optogenetic stimulation of the VTA-DA neurons (named oDAS), which is known to be rewarding and reinforcing (*22*–*24*), can induce facial movements. An oDAS with 20 pulses at 20 Hz elicited facial movements at the rostral parts including whiskers and nose, but not around ears and eyes, in awake head-restrained mice (Fig. 2B). We therefore further analyzed oDAS-induced whisker and nose movements by monitoring the frontal face of mice from a top view (Fig. 2, C to J, and movie S1). Our strongest oDAS with 20 pulses at 20 Hz induced rhythmic whisking with a high probability (83.8 ± 8.5 %, n = 7 mice; Fig. 2E). The average whisker angle during oDAS was protracted by 11.6 ± 2.6 degrees (n = 7 mice, 20 pulses at 20 Hz; Fig. 2F). The probability of whisking initiation, ΣWM during oDAS, and the average and maximum amplitude of whisker movements all increased, depending on the stimulus frequency (Fig 2, D to F) and photo-stimulus intensity (fig S2, A and B). In contrast, in control Ai32 mice without ChR2-expression, photostimulation of VTA did not evoke any consistent whisker movements (Fig. 2, D to F, and fig S2). Such protracted rhythmic whisking evoked by oDAS resembled whisker movements upon reward acquisition in reward-based learning tasks (Fig. 1, B and E). The oDAS-induced whisking had an average latency of 402 ± 51 ms (n = 7 mice, with 20 pulses at 20 Hz; Fig. 2J), which was significantly longer than the onset latency of whisking after optogenetic stimulation of the neurons in wM1 (145 ± 57 ms, n = 6, p = 0.0064, unpaired *t* test, Fig. 2J; *31*).

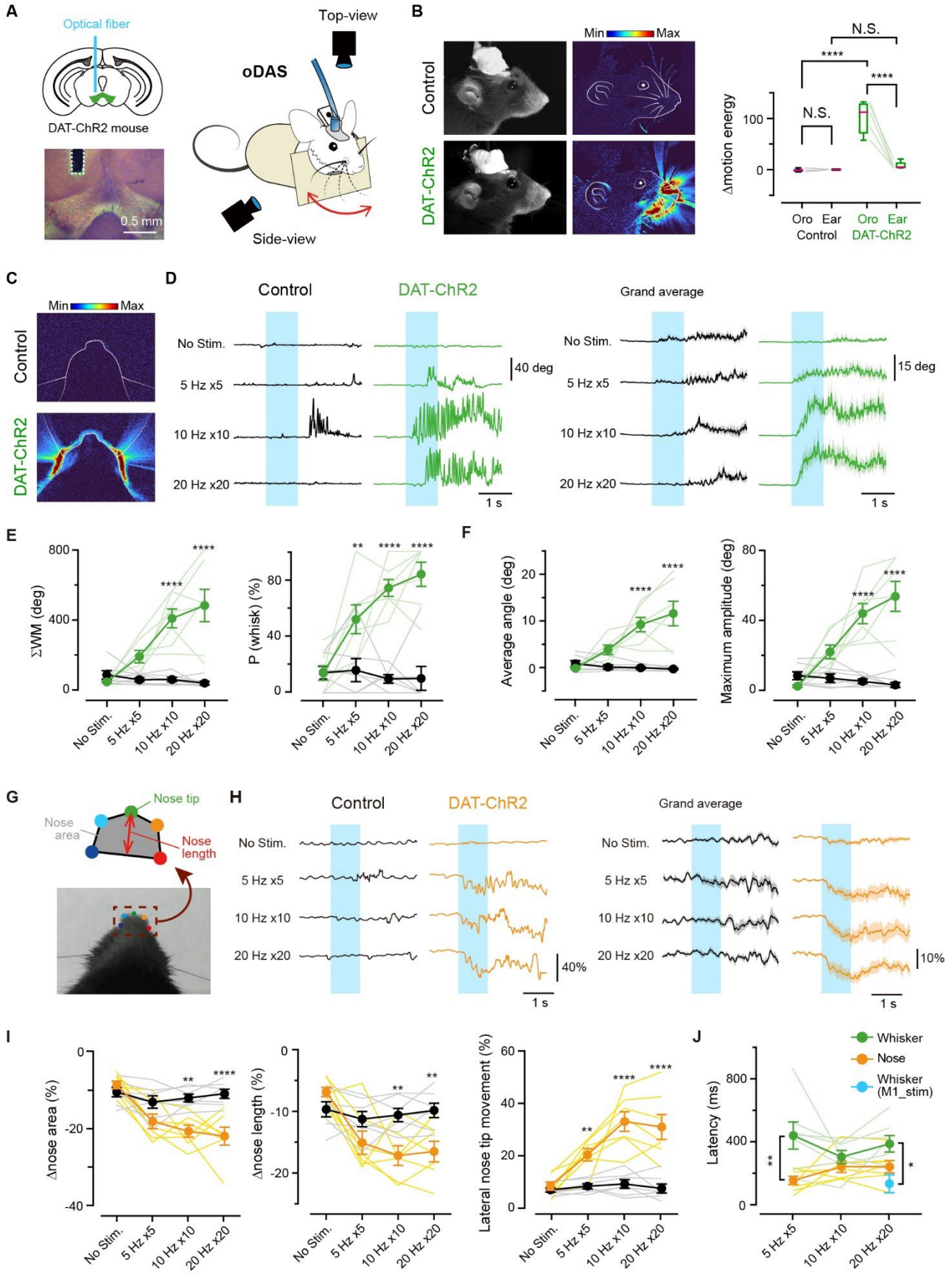
A
Optical fiber
DAT-ChR2 mouse
0.5 mm
oDAS
Top-view
Side-view
B
Min
Max
Control
DAT-ChR2
N.S.
****
N.S.
****
Δmotion energy
100
0
Oro
Ear
Control
Oro
Ear
DAT-ChR2
C
Min
Max
Control
DAT-ChR2
D
Control
DAT-ChR2
Grand average
No Stim.
5 Hz x5
10 Hz x10
20 Hz x20
40 deg
15 deg
1 s
E
ΣWM (deg)
P (whisk) (%)
No Stim.
5 Hz x5
10 Hz x10
20 Hz x20
F
Average angle (deg)
Maximum amplitude (deg)
G
Nose tip
Nose area
Nose length
H
Control
DAT-ChR2
Grand average
40%
10%
I
Δnose area (%)
Δnose length (%)
Lateral nose tip movement (%)
J
Whisker
Nose
Whisker (M1_stim)
Latency (ms)

Fig. 2. Orofacial movements induced by transient activation of VTA-DA neurons. (**A**) Left, schematic for the optical fiber location for the oDAS experiments (top), and an epifluorescence image of a coronal section containing VTA and the trace of the inserted fiber (dashed line) (bottom). Green: ChR2-eYFP, red: tyrosine hydroxylase, blue: DAPI. Rignt, schematic for the oDAS experiment. (**B**) Left, single example video frames from individual mice. Middle, motion energy heat-maps overlayed onto the face line drawings from the mice shown in Left. Right, quantifications for motion energy around the orofacial part (Oro) and the ear during oDAS. Medians of the box plots are shown in red. (**C**) Example motion energy heat-maps overlayed onto the top-view face line. (**D**) Left, example traces of the whisker position upon oDAS (light blue shadow) with different stimulus frequencies, obtained from a control (black) and DAT-ChR2 (green) mouse. Right, grand average of the whisker position upon oDAS (control: n = 7 mice; DAT-ChR2: n = 7 mice). Shadows of traces: ± SEM. (**E**) ΣWM (left) and P(whisk) (the probability of whisking initiation, right) during oDAS. (**F**) Average (left) and maximal (right) amplitude of whisker protraction (WP) angle during oDAS. (**G**) Schematic for the nose analysis (top) and a top-view snapshot of mouse face (bottom). (**H**) Same as (B) but for traces of the top-view nose area from control (black) or DAT-ChR2 (orange) mice. (**I**) Quantifications for the changes in nose area (left), nose length in the anterior-posterior axis (middle), and lateral movements of the nose tip (right). (**J**) Latencies of movement of the whisker (green) and nose (orange) upon oDAS. Filled circles and error bars show mean ± SEM. Lightly colored lines correspond to individual data. *$p < 0.05$, **$p < 0.01$, ***$p < 0.001$, ****$p < 0.0001$, N.S.: not significant, Bonferroni's multiple comparison test, control vs. DAT-ChR2 (E, F, and I) or whisker vs. nose (J).

We next analyzed nose movements evoked by oDAS using a deep learning-based toolbox DeepLabCut (*40*) (Fig. 2G). Mice exhibited nose twitches upon oDAS: the top-view nose area decreased (peak change from baseline: 22.0 ± 2.3%, n = 7) (Fig. 2, H and I), and the nose length in an anterior-posterior axis became shortened (peak change from baseline: 16.5 ± 1.6%, n = 7) (Fig. 2I), indicating contractions of the nasal muscle. The oDAS also induced a lateral movement of the nose tip (peak lateral movement as the percentage of the mean baseline nose length: 31.0 ± 4.8%, n = 7) (Fig. 2I). The magnitude of such nose movements depended on the stimulus frequency (Fig. 2, H and I) and photo-stimulus intensity (fig S2, C and D). Upon oDAS stimulation, nose and whisker movements were highly

correlated (fig. S3). The latencies of nose movement initiation and whisking initiation were similar, except for when using the weakest stimulation (Fig. 2J). Thus, transient activation of VTA-DA neurons is sufficient to facilitate movements in the whisker and nose. In contrast, optogenetic stimulation of DA neurons in the substantia nigra pars compacta (SNc), which are not normally related to reward processing but implicated in coordination of locomotion in mice (*41*, *42*), did not induce whisker and nose movements (fig. S4).

Reward-expecting cue-locked orofacial movements

In our liquid reward-based tasks, the cue-locked whisker protraction was immediately followed by anticipatory licking (Fig. 1E and fig S1, C to F). We next examined whether the cue-locked whisker protraction can be induced without anticipatory licking. We presented a sound cue (5 s) paired with oDAS during the last 1 s of the cue to head-restrained DAT-ChR2 or control (Ai32) mice (Fig. 3, A and B). Mice experienced ~20 trials of the paired stimulation per day, with random intertrial intervals between 180 and 240 s. On the first day of this conditioning (day 1), both DAT-ChR2 and control mice similarly exhibited a whisker protraction immediately after the sound presentation with a high probability (Fig. 3C), which might represent a reflex motor action to a salient auditory stimulus as observed in the auditory Go/No-Go task (fig S1, A and B). On day 2, however, DAT-ChR2 mice exhibited a rapid, cue-locked whisker protraction (24.3 ± 1.6 deg, n = 26 mice) (Fig. 3B) with a significantly larger amplitude than that on day 1 (18.3 ± 1.3 deg, n = 26 mice, $p < 0.0001$, Bonferroni's multiple comparison test; Fig. 3C). The amplitude of the cue-locked whisker protraction continued to increase over four days of learning (fig. S5A). In contrast, in control mice, the amplitude and probability of the cue-locked whisker protraction significantly decreased on day 2 (Fig. 3, B and C). These results indicate that learning the sound-oDAS pairing can elicit cue-locked

whisker protraction even in absence of goal-directed action. The latency of whisker protraction after the onset of the sound presentation was 98 ± 7 ms (n = 26 mice) on day 2 (Fig. 3G), which was significantly shorter than that of oDAS-induced whisker motion ($p < 0.0001$, with 20 pulses at 20 Hz, Mann-Whitney *U* test, Fig. 2J) and similar to the latency of whisking after optogenetic wM1 stimulation ($p = 0.87$, Mann-Whitney *U* test, Fig. 2J). In addition to the whisker protraction, a quick nose twitch was also elicited immediately after the sound onset in DAT-ChR2 mice on day 2 (peak change in the nose area: 25.1 ± 2.2%, n = 26 mice; peak change in the nose length: 22.2 ± 2.0%, n = 26 mice; peak lateral movement of the nose tip: 36.1 ± 2.2%, n = 26 mice), which was absent in control mice without ChR expression on day2 (Fig. 3, D to F). The latency of the cue-locked nose twitch (156 ± 10 ms, n = 26 mice) was significantly longer than that of the cue-locked whisker protraction ($p = 0.0008$, two-way ANOVA; Fig. 3G) but still shorter than that of oDAS-induced nose movement (257 ± 38 ms, upon oDAS at 20 Hz for 1 s, n = 7 mice, $p = 0.0006$, unpaired *t* test). The amplitudes of the nose twitch and whisker protraction at the cue onset were weakly but significantly correlated (fig. S6). Control mice showed small reflex movements in the whisker and nose at the cue onset in a small fraction of the trials on day 1 (Fig. 3, C, E and F). Its amplitude and probability significantly decreased with training (Fig. 3, C, E and F), suggesting that the cue-locked orofacial motions in the early stage of our sound-reward conditioning tasks might also include the response to a salient auditory stimulus. Thus, the cue-locked orofacial movements at the later stage of reward-based learning should mainly represent the internal states of reward expectation. In this sound-oDAS association task, we also observed oDAS-aligned whisker movements (Fig. 3B). The magnitude of whisker movements and the probability of whisking during oDAS in this task did not change over five days, with a slight tendency to be attenuated after three days, although not statistically significant (fig. S5B).

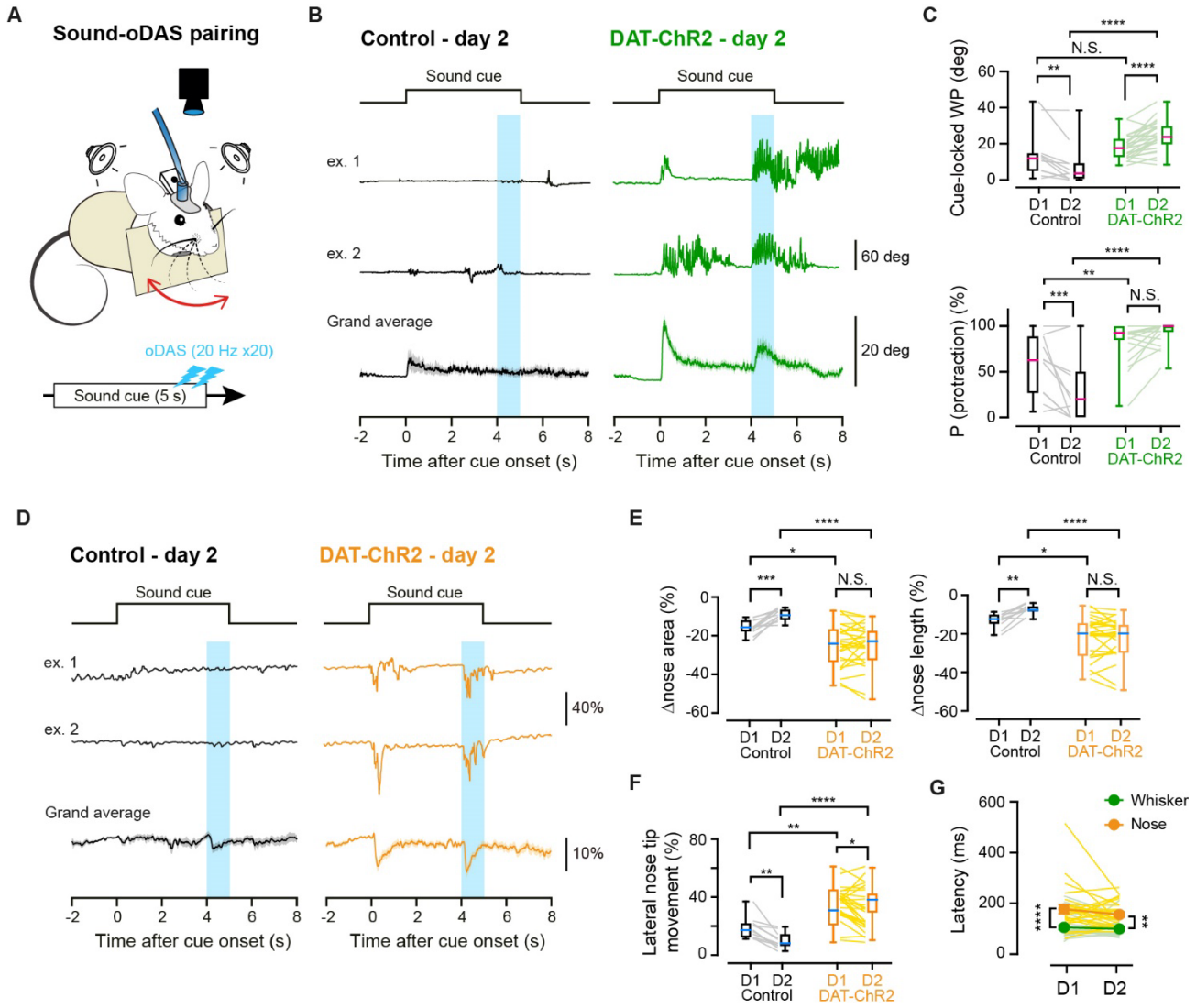

Fig. 3. Orofacial movements during a stimulus-oDAS association task. (**A**) Schematic for the sound-oDAS pairing conditioning. (**B**) Example and grand average traces of the whisker position during the sound-oDAS pairing conditioning on day 2, obtained from a control (black) and DAT-ChR2 (green) mouse (control: n = 11 mice; DAT-ChR2: n = 26 mice). The timings of the sound cue presentation (black line) and oDAS (light blue shadow) are indicated. Shadows of grand average traces: ± SEM. (**C**) The amplitude of cue-locked whisker protraction (WP, top) and P(protraction) (protraction probability, bottom) on day 1 (D1) and day 2 (D2). (**D**) Same as (B) but for traces of the top-view nose area from control (black) or DAT-ChR2 (orange) mice. (**E** and **F**) Quantifications for the changes in nose area (left in E), nose length (right in E), and the changes in lateral movements of the nose tip (F). (**G**) Latencies of cue-locked whisker protraction (green) and nose tip movements (orange) upon sound cue presentation. Medians of the box plots are shown in magenta (C) or cyan (E and F).

Filled circles and error bars in (G) show mean ± SEM. Lightly colored lines correspond to individual data. *p < 0.05, ** p < 0.01, N.S., ***p < 0.001, ****p < 0.0001, N.S.: not significant, two-way ANOVA followed by Bonferroni's multiple comparison test, whisker vs. nose (G).

Involvement of accumbal D1R in driving orofacial movements

We next investigated the neuronal circuits downstream of VTA DA neurons for inducing reward-related orofacial movements. Stimulation of VTA DA neurons is known to activate medium spiny neurons expressing D1 receptors (D1Rs) in the nucleus accumbens (NAc) through the mesolimbic DA pathway (*43*). We therefore examined the role of D1Rs in reward-related orofacial movements. Intraperitoneal (IP) injection of a D1 receptor (D1R) antagonist, SCH23390 (0.3 mg/kg), abolished the oDAS-induced whisking (ΣWM: saline = 487 ± 127 deg [n = 7 mice], SCH23390 = 32.4 ± 5.3 deg [n = 7 mice], p = 0.013, paired *t* test; whisking probability: saline = 81.6 ± 11.2% [n = 7 mice], SCH23390 = 5.4 ± 5.4% [n = 7 mice], p = 0.031, Wilcoxon signed rank test) and nose twitches (peak change in the nose area: saline = 25.0 ± 5.5% [n = 7 mice], SCH23390 = 5.0 ± 1.3% [n = 7 mice], p = 0.011, paired *t* test) in DAT-ChR2 mice (Fig. 4, A and B, and fig S7A), suggesting the involvement of D1Rs. The IP injection of SCH23390 also reduced the spontaneous whisker movements (ΣWM per a second: saline = 159 ± 25 deg/s [n = 9 mice], SCH23390 = 55.2 ± 8.1 deg/s [n = 9 mice], p = 0.0058, paired *t* test; Fig. 4A), suggesting a general sedative effect of the D1R antagonist. To specifically examine the role of D1Rs in the NAc in driving oDAS-induced orofacial movements, we used CRISPR-Cas9-mediated *in vivo* genome editing. We knocked out D1Rs in the NAc of DAT-ChR2 mice by local injection of an AAV vector harboring saCas9 with guide RNA targeting the first transmembrane domain of *Drd1a* (AAV-gRNA), which has been previously shown to have a high cleavage rate and no off-target effects (*44*) (Fig. 4C and fig S7, B and C). These NAc-D1R-KO mice did not show whisker movements or nose twitches

upon oDAS (Fig. 4, C and D, and fig S7D). In contrast, control mice injected with a control AAV saCas9-gRNA vector (AAV-Control) exhibited oDAS-induced whisker movements and nose twitches (Fig. 4, C and D, and fig S7D). Spontaneous whisker movements were unaffected in NAc-D1R-KO mice (Fig. 4C). These results suggest the involvement of accumbal D1Rs in oDAS-induced orofacial movements. Moreover, optogenetic activation of the axons of VTA-DA neurons in the NAc induced whisker movements and nose twitches (Fig. 4, E and F, and fig S7E). Our results thus indicate that the mesolimbic DA pathway mediates oDAS-induced orofacial movements through activation of D1Rs in the NAc.

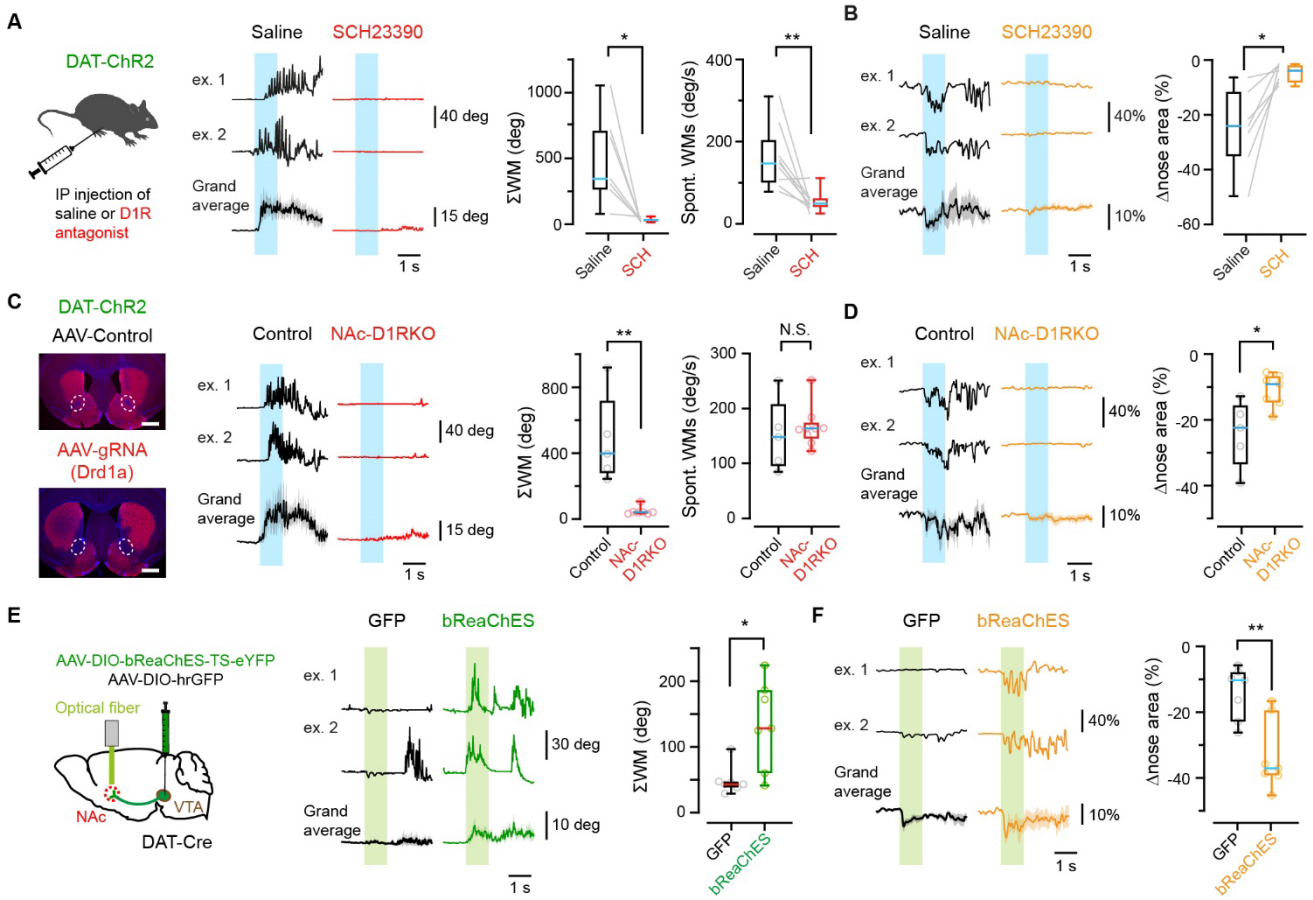

Fig. 4. Essential involvement of accumbal D1Rs in oDAS-induced orofacial movements. (**A**) Left, schematic for the experiment. Middle, example and grand average traces of the whisker position

upon oDAS (light blue shadow) in trials with IP injection of SCH23390 (red) and saline (black). Right, ΣWM during oDAS and the magnitude of spontaneous whisker movements (WMs) (n = 7 mice). (**B**) Example and grand average traces (left) and quantifications (right) of the top-view nose area in trials with IP injection of saline (black) or SCH23390 (orange). (**C**) Left, epifluorescence images of coronal sections containing NAc (dashed circles) from mice with bilateral injection of control AAV (top) or AAV with guide RNA targeting Drd1a (bottom). Red, Drd1, blue: DAPI, Scale bar: 1 mm. Middle, example and grand average traces of the whisker position in NAc-D1R-KO (red) and control (black) mice upon oDAS. Right, ΣWM and the magnitude of the spontaneous WMs during oDAS (control: n = 5 mice; NAc-D1R-KO: n = 7 mice). (**D**) Same as (B) but for data from NAc-D1R-KO (orange) and control (black) mice. (**E**) Left, schematic for the optogenetic experiment. Middle, example and grand average traces of the whisker position upon oDAS in bReaChES- (green) and GFP- (black) expressing mice. Right, data for each mouse (thin lines) and box plots for the ΣWM during oDAS (n = 7 mice for each). (**F**) Same as (B) but for data from bReaChES- (orange) and GFP- (black) expressing mice. Green shadow: stimulation timing. Medians of the box plots are shown in magenta (E) or cyan (A–D and F). Shadows of grand average traces: ± SEM. Open circles and lightly colored lines correspond to individual data. *$p < 0.05$, ** $p < 0.01$, N.S.: not significant, paired *t* test (A and B), Mann-Whitney U test (ΣWM in C and E) or unpaired *t* test (Spont. WMs in C, D and F).

We further tested whether D1Rs are also involved in generating the cue-locked whisker protraction. We performed an IP injection of saline or SCH23390 in the mice that had learned the sound-oDAS pairing for two days and analyzed orofacial movements upon the paired stimulation on the third day. Even though the IP injection of SCH23390 dramatically reduced spontaneous and oDAS-induced whisker movements (Fig. 4A), it did not affect the cue-locked whisker protraction after learning of the sound-oDAS pairing (cue-locked whisker protraction amplitude: saline = 33.8 ± 4.4 deg [n = 6 mice], SCH23390 = 30.0 ± 4.0 deg [n = 6 mice], p = 0.35, paired *t* test) (Fig. 5, A and B). The D1R antagonist did also not significantly attenuate nose twitches time-locked to the sound cue (peak change in the nose area: saline = 24.0 ± 3.7 deg [n = 6 mice], SCH23390 = 18.3 ± 3.4 deg [n = 6 mice], p = 0.20, paired *t*

test) (Fig. 5, C and D). Thus, the oDAS-induced and cue-locked orofacial movements are differentially driven by D1R-dependent and -independent neuronal circuits, respectively.

We further tested whether another DA receptor, D2 receptor (D2R), is involved in cue-locked orofacial movements. IP injection of SCH23390 together with a D2R antagonist, raclopride (3 mg/kg) did not affect cue-locked whisker movements (fig. S8, A and B), but it largely attenuated the cue-locked nose movements (fig. S8, C and D). These results suggest that D2Rs regulate whisker and nose movements differentially in response to reward-predicting cue presentation.

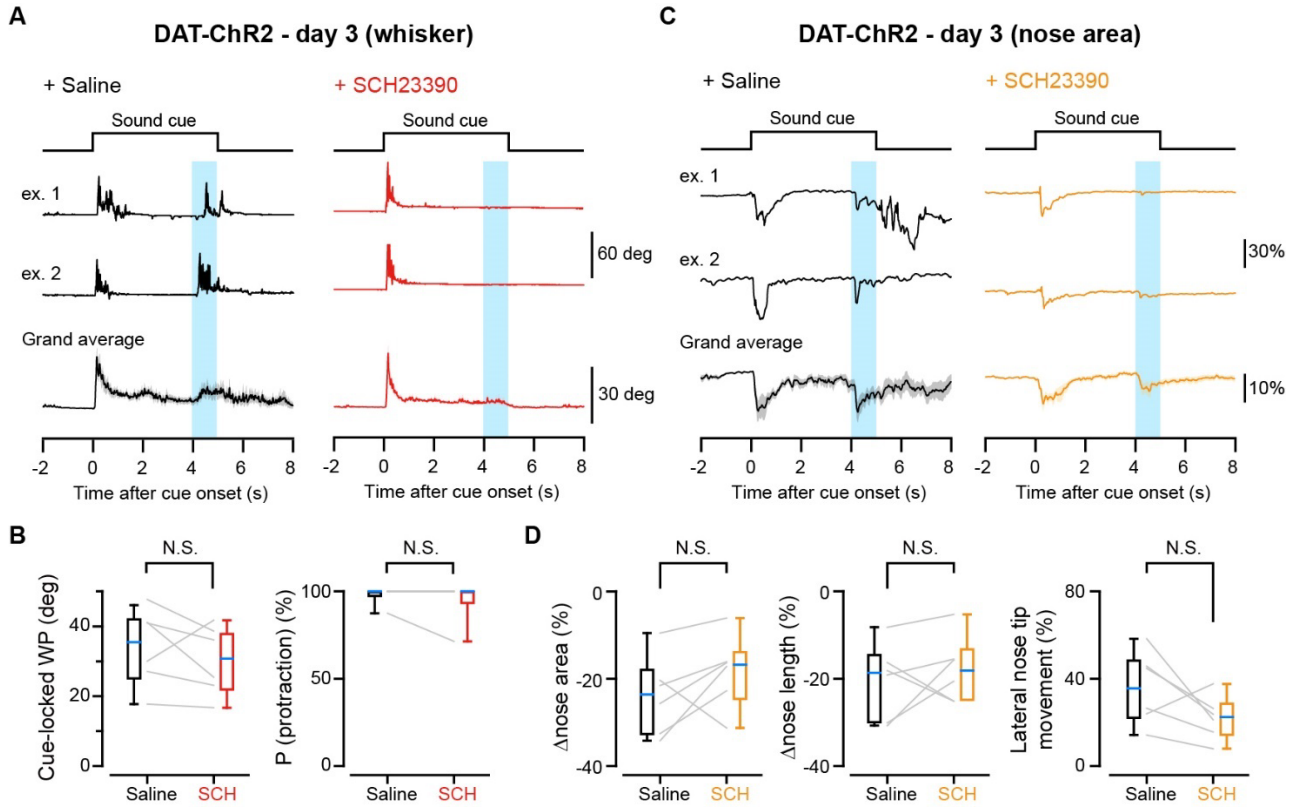

Fig. 5. Orofacial movements upon reward expectation do not require D1Rs. (**A**) Example and grand average traces of the whisker position in trials with SCH23390- (red) or saline- (black) injection in DAT-ChR2 mice during sound-oDAS pairing experiments on day 3 (n = 6 mice). The timings of the sound cue presentation (black line) and oDAS (light blue shadow) are indicated. Shadows of grand

average traces: ± SEM. (**B**) The amplitude of cue-locked whisker protraction (WP, left) and protraction probability (right) upon sound cue presentation. (**C**) Same as (A) but for traces of the top-view nose area. (**D**) Same as (B) but for the parameters of nose movement. Medians of the box plots are shown in cyan. Thin lines correspond to individual data. N.S.: not significant, paired *t* test (Cue-locked WP in B and D) or Wilcoxon signed rank test (P(protraction) in B).

Whisker M1 drives reward-related orofacial movements

Mouse whisker primary motor cortex (wM1) plays a critical role in triggering exploratory whisking (*29*, *31*). Having identified D1R-independent neuronal circuits driving the cue-locked orofacial movements, we next examined the involvement of wM1 in reward-related orofacial movements using DAT-ChR2 mice. Silencing of wM1 by injection of muscimol (5 mM in Ringer's solution, total 400 nl), a $GABA_A$-receptor agonist, led to a dramatic drop in the magnitude and probability of oDAS-induced whisker movements (ΣWM: before muscimol = 243 ± 40 deg [n = 6 mice], after muscimol = 55.0 ± 12.0 deg [n = 6 mice], p = 0.0095, paired *t* test; whisking probability: before muscimol = 59.9 ± 6.1% [n = 6 mice], after muscimol = 17.1 ± 6.4% [n = 6 mice], p = 0.0027, paired *t* test) (Fig. 6, A and B). Inactivation of wM1 by muscimol also attenuated oDAS-induced nose twitches (peak change in the nose area: before muscimol = 24.2 ± 1.6% [n = 6 mice], after muscimol = 5.6 ± 1.3% [n = 6 mice], p = 0.0001, paired *t* test; Fig. 6, C and D, and fig S9A). Injection of Ringer's solution in wM1 did not affect these oDAS-induced orofacial movements (Fig. 6, B and D, and fig S9A). Thus, neuronal activity in wM1 is required for the generation of oDAS-induced orofacial movements.

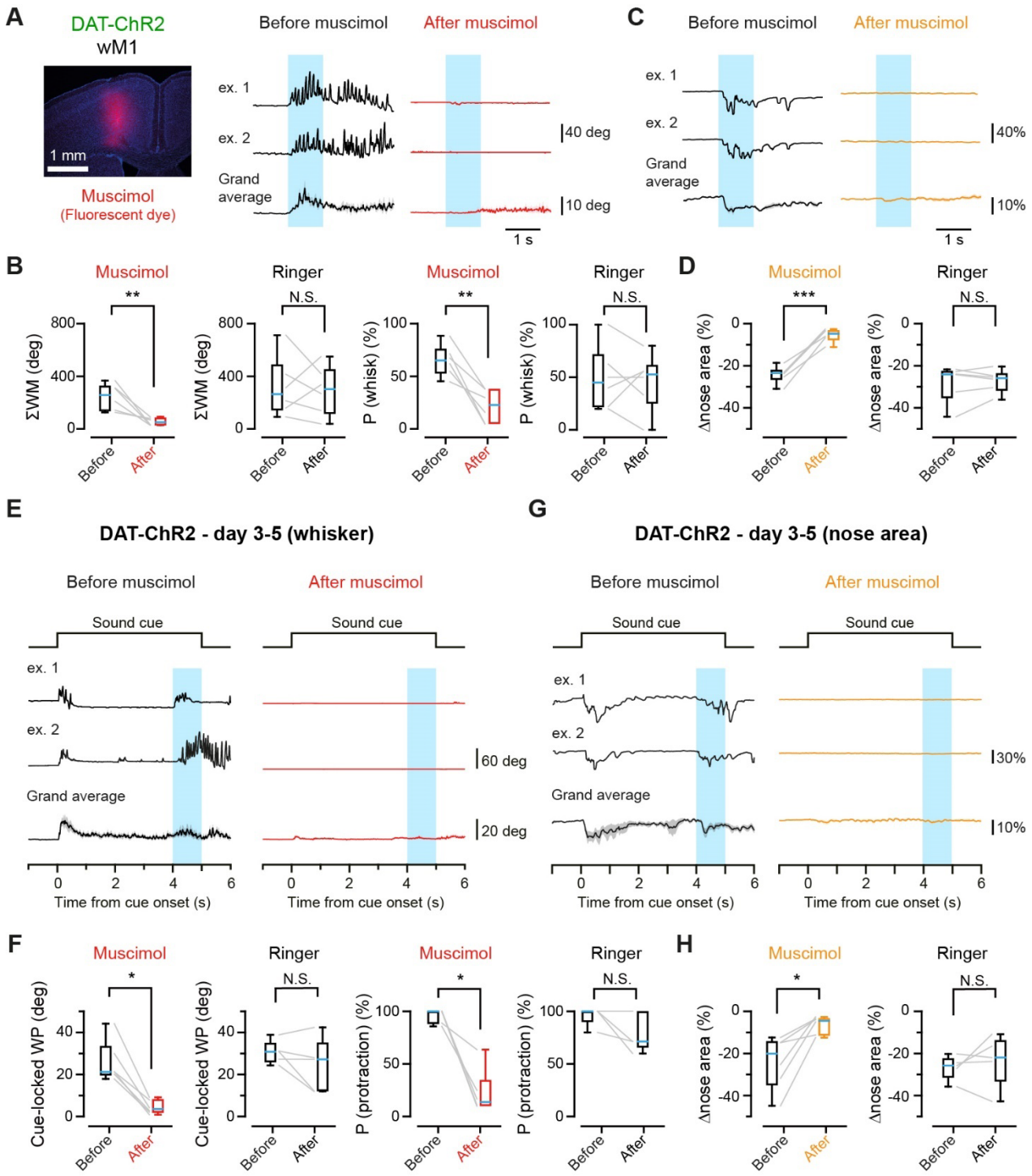

Fig. 6. Dominant role of wM1 in driving reward-related orofacial movements. (**A**) Left, an epifluorescence image of a coronal section indicating the muscimol injection site. A small volume of Chicago sky blue (red) was dissolved into the vehicle. Blue: DAPI Right, example and grand average

traces of the whisker position upon oDAS (light blue shadow) before (black) and after (red) muscimol injection in wM1 of DAT-ChR2 mice (n = 6 mice). (**B**) ΣWM and the probability of whisking initiation in trials before (black) and after (red) injection of muscimol or Ringer's solution (n = 6 mice for each). (**C**) Example and grand average traces of the nose area before (black) and after (orange) muscimol injection into wM1. (**D**) Same as (B) but for the nose area. (**E**) Example and grand average traces of the whisker position before (black) and after (red) muscimol injection into wM1 of DAT-ChR2 mice during sound-oDAS pairing experiments. (**F**) Same as (B) but for the amplitude and occurrence probability of cue-locked whisker protraction (WP) during sound-oDAS pairing experiments (muscimol, n = 6 mice; Ringer, n = 5 mice). (**G** and **H**) Same as (E and F) but for nose area. Medians of the box plots are shown in cyan. Thin lines correspond to individual data. Shadows of grand average traces: ± SEM. *p < 0.05, **p < 0.01, ***p < 0.001, N.S., not significant, paired *t* test (all of B, D and H and cue-locked WP for Ringer in F) or Wilcoxon signed rank test (two panels for Muscimol and P(protraction) for Ringer in F).

We further investigated whether the cue-locked orofacial movements during the sound-oDAS pairing stimuli also depend on wM1 activity. We used DAT-ChR2 mice that learned the sound-oDAS pairing for 2–4 days and tested injection of muscimol or Ringer's solution into wM1 on the next day. Inactivation of wM1 by muscimol largely attenuated the cue-locked whisker protraction (amplitude: before muscimol = 25.8 ± 4.0 deg [n = 6 mice], after muscimol = 4.6 ± 1.4 deg [n = 6 mice], p = 0.031, Wilcoxon signed rank test; probability: before muscimol = 95.8 ± 2.7% [n = 6 mice], after muscimol = 22.7 ± 8.5% [n = 6 mice], p = 0.031, Wilcoxon signed rank test; Fig. 6, E and F) and nose twitch (peak change in the nose area: before muscimol = 24.0 ± 5.2% [n = 6 mice], after muscimol = 6.5 ± 1.7% [n = 6 mice], p = 0.013, paired *t* test; Fig. 6, G and H, and fig S9B). Injection of Ringer's solution did not affect the cue-locked orofacial movements (Fig. 6, F and H, and fig S9B). Our results thus suggest that wM1 activity is crucial for the generation of both oDAS-induced and cue-locked orofacial movements.

Representation of reward-related orofacial movements in wM1

wM1 thus appears to have a dominant role in driving both oDAS-induced and cue-locked orofacial movements which presumably reflect the internal states of reward acquisition and reward expectation, respectively. Therefore, it is of interest to investigate the neuronal signals in wM1 during reward-related facial movements. Using multisite silicone probes, we measured the action potential firing in wM1 of head-restrained DAT-ChR2 mice during stimulus-oDAS pairing stimulation, where both oDAS-induced (reward-acquiring) and cue-locked (reward-expecting) orofacial movements could be induced in single trials. We performed recordings in four DAT-ChR2 mice that had already experienced the stimulus-oDAS pairing conditioning for three days. The reward-related orofacial behaviors (the amplitude and probability of cue-locked whisker protraction and the magnitude and probability of oDAS-aligned whisker movements) of these mice on the recording day were essentially the same as those on day 2 (fig. S10). Among the 174 units we identified in wM1, 103 units (59.2 %) significantly increased or decreased their firing rate at the cue onset and/or during oDAS. To examine the correlation between the activity of individual neurons and whisker behavior, we first excluded trials where spontaneous whisking started during the pre-trial period (1 s) from analysis and then categorized trials based on the behavior (Fig. 7, A and B). In 20.8% of trials, both cue-locked whisker protraction and whisking during oDAS were observed (RE+RA trials, n = 4 mice). There were also trials with only cue-locked whisker protraction but not oDAS-aligned whisker movements (RE trials, 37.6%) and those with only oDAS-aligned whisker movements but not cue-locked whisker protraction (RA trials, 11.9%). We analyzed a correlation between neuronal activities and cue-locked whisker protraction amplitude in RE+RA and RE trials or variance of whisker position during oDAS in RE+RA and RA trials. We found the units specifically representing reward expectation (RE cells) with their

firing rate increased at the cue onset only when mice showed whisker protractions, while their firing rate did not correlate with oDAS-aligned whisker movements (Fig. 7, C, E and F). In contrast, those representing reward acquisition (RA cells) responded to oDAS only when mice showed oDAS-aligned whisker movements while showing no correlation with cue-locked whisker protractions (Fig. 7, D to F). There was also a population of wM1 units representing both cue-locked whisker protractions and oDAS-aligned whisker movements (RE+RA cells; Fig. 7, E and F). In our recording, 12.6% of the units were defined as RE cells, 9.8% as RA cells, and 3.4% as RE+RA cells (Fig. 7E). We further separated units into regular spiking (RS) and fast spiking (FS) units, according to their trough-to-peak time of average spike waveform (fig. S11A). We found no apparent specificity in the fraction of FS cells in these RE and RA cells (fig. S11, B and C) and other stimulus-modified neurons (fig. S11D). Our results thus suggest that wM1 contains specific neuronal populations that signal the internal states related to reward expectation and reward acquisition.

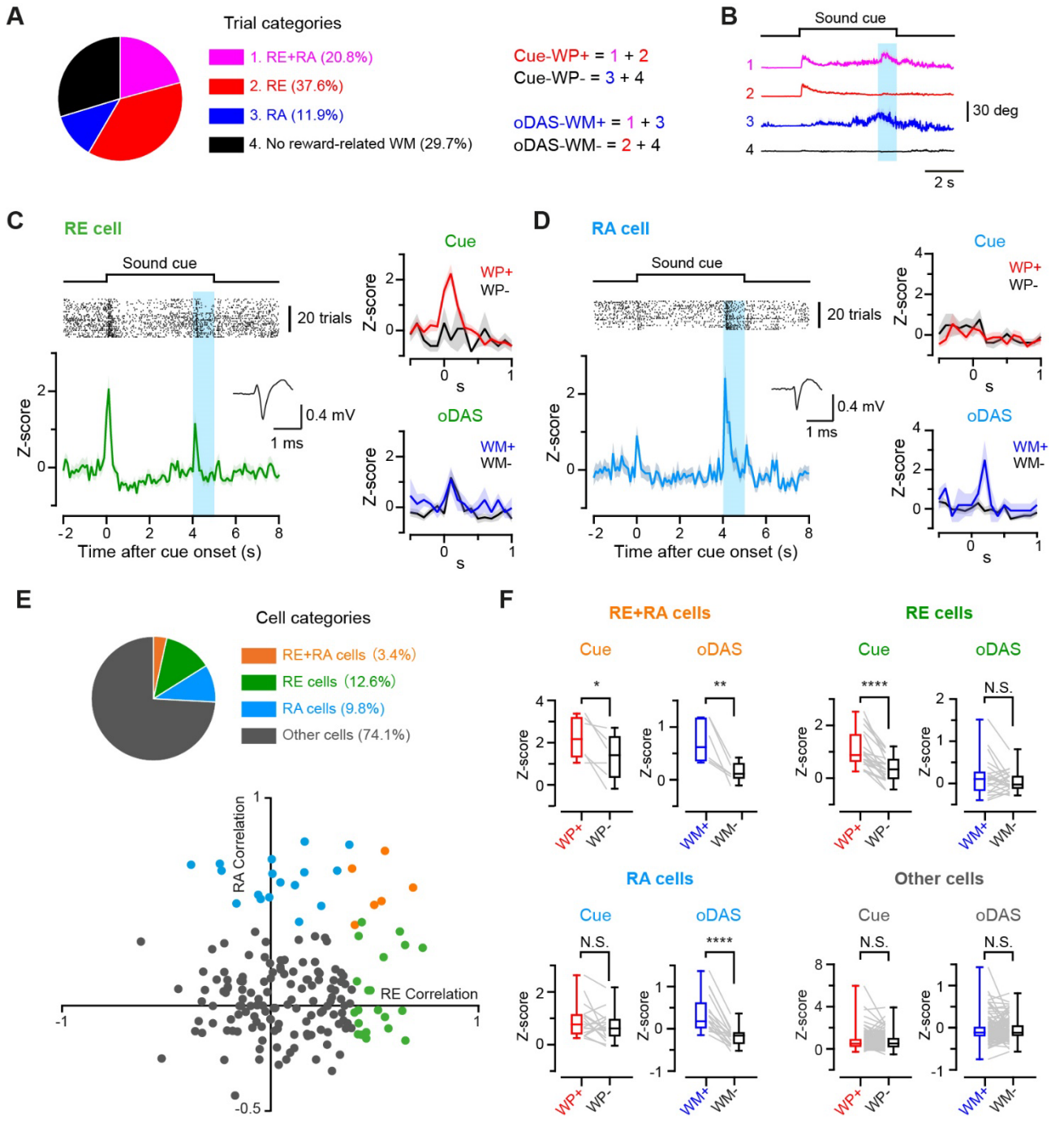

Fig. 7. Neuronal correlates of cue-locked and oDAS-induced whisker movements in wM1. (**A**) Summary of the trial categories. (**B**) Grand average traces of the whisker position in trial categories indicated in (A). (**C**) Left, example raster plot (top) and corresponding Z-scored peri-stimulus time histogram (PSTH, bottom) obtained from a representative RE cell. The averaged action potential waveform is shown in the inset. Right, Z-scored PSTH of the same cell at around the cue onset (top)

and upon oDAS (bottom), comparing data with or without whisker protraction at the cue onset or whisker movement during oDAS. (**D**) Same as (C) but for a representative RA cell. (**E**) Top, summary of the cell categories. Bottom, scatter plot containing 174 neurons from four mice experiencing the sound-oDAS pairing stimulation on the fourth day of conditioning, plotted on the basis of their correlation to the ΣWM during oDAS (RA correlation) and the cue-locked whisker protraction amplitude (RE correlation). Subsets of neurons showing significant, positive correlation are colored in orange (RE+RA cell), green (RE cell) or cyan (RA cell). (**F**) Z-scored average firing rate of each cell category at the cue onset (Cue) or during oDAS (oDAS), comparing data with or without whisker protraction at the cue onset or whisker movement during oDAS. A thick line and shadows in (C) and (D) indicate mean ± SEM. *$p < 0.05$, **$p < 0.01$, ****$p < 0.0001$, N.S., not significant, paired *t* test (for RE+RA cells) or Wilcoxon signed-rank test (for RE, RA, and Other cells).

DISCUSSION

Through high-speed filming of orofacial movements of head-restrained mice performing reward-based learning tasks, we have characterized expressive facial movements at the timings of expectation and acquisition of a reward. We found stereotypical movements in the whisker and nose representing reward expectation and acquisition and identified neuronal correlates of these movements in mouse wM1. Previous studies showing task-aligned uninstructed orofacial movements (*9*–*13*) used tasks involving motor actions for execution, such as holding handles, locomotion, and licking. Using a Pavlovian learning paradigm, we demonstrated that mice exhibit reward-related orofacial movements even without any need for motor action. Given that orofacial motion energy correlates well with brain-wide neuronal activity (*10*, *12*, *45*), the reward-related orofacial movements may shape neuronal activities in different regions of the brain.

In our stimulus-reward association tasks, the cue-locked whisker protraction is induced before the initiation of goal-directed or anticipatory licking. A whisker protraction with similar kinetics can be elicited even without licking in our stimulus-oDAS pairing task,

suggesting that the cue-locked whisker protraction reflects the generalized internal states of reward expectation. The mean amplitude of cue-locked whisker protraction increases as the mice learn the tasks, indicating the scalability of the behavior corresponding to the magnitude of reward expectation. Such generality and scalability of the behavior suggest that the cue-locked whisker protraction is not merely a reflexive movement upon salient stimuli. A quick nose twitch is often coupled to the cue-locked whisker protraction in the stimulus-oDAS pairing task. These highly reproducible cue-locked orofacial movements appeared only transiently, followed by more random movements in the whisker and nose at the later phases of the cue presentation. Our observations are in line with the studies showing increased body and facial activities, including enhanced locomotion and sniffing at a higher frequency upon reward expectation (*11*, *46*–*49*). A classical study (*50*) described a stereotypical movement sequence during a sniffing cycle, starting with head fixation, whisker protraction, a brief inhalation, and retraction of the tip of the nose. Therefore, the cue-locked whisker protraction and quick nose twitch described in the present study may correspond to a single sniffing cycle.

Facial expressions in mice can appear in the ears, eyes, cheeks, and nose (*5*–*8*). However, facial movements evoked by oDAS were restricted mainly in the orofacial parts (Fig. 2B). The oDAS-evoked active whisker movements have longer latency and are more persistent than the cue-locked whisker protraction, and generally have a protracted set point, similar to exploratory whisking (*29*, *31*). Nose twitches also accompany the oDAS-induced whisker movements, suggesting the occurrence of sniffing (*47*, *50*). Whisker movements upon oDAS show scalable positive correlations with the stimulus frequency (Fig. 2) and light intensity (fig. S2) of oDAS, that would be correlated to reward-prediction error signals in the brain (*18*, *25*–*27*, *51*). The significant kinetic differences in reward acquisition (Fig. 2J)- and

reward expectation (Fig. 3G)-related motions suggest that different neuronal circuits drive these two types of orofacial movements.

Whisker movements are driven by facial muscles innervated by cholinergic motor neurons in the lateral facial nucleus. These whisker motor neurons receive synaptic inputs from premotor neurons, which are distributed in multiple areas within the brain stem, the midbrain, and the neocortex (for reviews, *52*, *53*). Although there are significant kinetic differences in reward acquisition- and reward expectation-related motion, whisking and nose movements often occur simultaneously. The respiratory centers in the ventral medulla that coordinate whisking and sniffing are thus likely involved in reward-related orofacial movements (*16*). Our perturbational analyses indicate that VTA-DA neurons could directly or indirectly regulate the activity of these premotor circuits. Accumbal D1Rs are indispensable for the oDAS-induced, reward-acquiring orofacial movements (Fig. 4). D1R-expressing GABAergic neurons in the NAc (NAc-D1R neurons) have outputs to the substantia nigra pars reticulata (SNr) which contains GABAergic neurons projecting to motor-related nuclei of the thalamus (motor thalamus). Activation of NAc-D1R neurons by oDAS thus leads to activation of the motor thalamus and, subsequently, the motor cortex. We found that neuronal activities in wM1 are essential for generating oDAS-induced whisker movements (Fig. 6) and identified specific neuronal populations that respond to oDAS in wM1 (Fig. 7). Considering that wM1 is also crucial for triggering exploratory whisking (*29*, *31*) and that oDAS-induced whisking is quantitatively indistinguishable from exploratory whisking, we hypothesize that multi-nuclei transmission of reward information from VTA to wM1 might have a dominant role in driving the overt facial expressions of reward acquisition in mice. The wM1 strongly innervates brain stem reticular nuclei containing whisker premotor neurons, which may form a central pattern generator for rhythmic whisking (*29*, *30*). However, we cannot exclude the possibility that

signals from NAc-D1R neurons through pathways independent of wM1 might also contribute to the activation of motor neurons in the facial nucleus.

The transient whisker protraction upon reward expectation is reminiscent of transient firings of VTA DA neurons and subsequent DA release in the NAc immediately after reward-predicting cue presentation (*25*–*27*, *54*). DA released in the NAc would activate D1R-expressing neurons generating the signal flow towards wM1 as discussed above. However, our results show that D1Rs do not mediate the facial expressions of reward expectation (Fig. 5). We speculate that learning a stimulus-reward association might recruit a cortical sensorimotor-coupling for reward expectation signaling, thereby activating wM1 earlier than the signals through NAc-D1R neurons. Differences in the onset latencies (Fig. 3G) and the sensitivity to a D2R antagonist (fig. S8) suggest that the neuronal mechanisms of cue-locked nose twitches might differ from those of the cue-locked whisker protraction. In fact, the magnitudes of these two movements were only weakly correlated (fig. S6).

Although facial movements are roughly correlated with brain-wide activity (*10*, *12*, *45*), we found that different neuronal populations in wM1 represent reward expectation and reward acquisition (Fig. 7). The causal function of wM1 in forming facial expressions implies that these wM1 neurons representing reward-related orofacial movements may have a global impact on neuronal processing in the brain during reward-based behaviors through inducing motor-related brain state changes. On the other hand, our results disagree with the classical observation of intact tastants-evoked orofacial expressions in animals with chronic decerebration (*37*, *38*). Substantial rewiring of neuronal circuits may take over the function of ablated brain regions (*55*, *56*).

Our findings provided insights into the neuronal mechanisms of reward-related expressive orofacial movements. However, it is still enigmatic why mice move their whiskers

and nose upon reward expectation and acquisition. When mice feel rewarded, they may attempt to gather sensory information in their immediate surroundings to memorize the environment that might cause a rewarding experience. Another possibility would be that reward-related orofacial movements may be perceived by other conspecifics through social facial touches. Interindividual transmission of reward-related internal states may have a role in animals' prosocial behaviors. It will therefore be of critical importance to investigate how reward-related orofacial movements function in social communications.

MATERIALS AND METHODS

Animals

All experimental procedures were approved by the Swiss Federal Veterinary Office (for whisker detection task experiments), the institutional review board of the Research Institute of Environmental Medicine, Nagoya University, and the Institutional Animal Care and Use Committee of Fujita Health University. For optogenetic experiments, we used DAT-ChR2 mice by crossing DAT-IRES-Cre mice [B6.SJL-*Slc6a3*$^{tm1.1(cre)Bkmn}$/J] with Ai32 mice [B6;129S-*Gt(ROSA)26Sor*$^{tm32(CAG-COP4*H134R/EYFP)Hze}$/J] (*57*), Ai32 mice as control or DAT-IRES-Cre mice with AAV injected (see below). For behavioral experiments using water reward-based learning tasks (Fig. 1), we used adult male C57BL/6J wild-type mice. Mice were at least 6-week-old at the time of head-post implantation (see below). Mice were kept in a shifted light/dark cycle (light 0 p.m. to 0 a.m. in Nagoya University and Fujita Health University; light 7 p.m. to 7 a.m. in EPFL) in ventilated cages at a temperature of 23 ± 3°C with food available ad libitum. Behavioral experiments were performed during the dark period. Water was restricted during the training of water reward-based learning tasks. All mice were weighed

and inspected daily during behavioral training and given wet food, so that mouse weight was kept to be more than 80% of the initial value.

Plasmids

For AAV production, pAAV-Ef1a-DIO-bReaChES-TS-eYFP was obtained from K. Deisseroth (Stanford University). For CRSPR-Cas9-mediated gene editing, we used a plasmid containing a saCas9 encoding sequence with *Drd1a*-targeting short guide RNA (*44*): pairs of *Drd1a*-targeting oligo DNAs (forward, 5'-CACCGCTTATCCTGTCCACTCTCTTA-3', reverse, 5'-AAACTAAGAGAGTGGACAGGATAAGC-3') were ligated into a plasmid pX601-AAV-CMV::NLS-SaCas9-NLS-3xHA-bGHpA;U6::BsaI-sgRNA (Addgene #61591) digested with BsaI (New England BioLabs). We constructed a plasmid with negative-control saCas9 guide RNA by linearizing the saCas9-*Drd1a*-gRNA plasmid with BsaI (New England BioLabs) and ligating a pair of random DNA sequences having no any identical sequence in the mouse genome (forward, 5'-CACCGTCAATAATGAGGTGGTCCGA-3'; reverse, 5'-AAACTCGGACCACCTCATTATTGAC-3') with T4 DNA Ligase (New England BioLabs).

Viral production

To produce AAV vectors for axonal stimulation experiments (Fig. 4, E and F), HEK293 cells were transfected with vector plasmids including pAAV encoding bReaChES or hrGFP together with pHelper, and pAAV-RC (serotype 9 or DJ), using a standard calcium phosphate method. After three days, transfected cells were collected and suspended in lysis buffer (150 mM NaCl, 20 mM Tris pH 8.0). After four freeze-thaw cycles, the cell lysate was treated with 250 U/ml benzonase nuclease (Merck) at 37 °C for 10–15 min with adding 1 mM $MgCl_2$ and then centrifuged at 4 °C at 1753×g for 20 min. AAV was then purified from the supernatant

by iodixanol gradient ultracentrifugation. The purified AAV solution was concentrated in PBS via filtration and stored at −80°C.

For *in vivo* genome editing experiment (Fig. 4, C and D), HEK293 cells were transfected with vector plasmids including pAAV encoding *Drd1a*-targeting guide RNA or control guide RNA, together with pHelper, and pAAV-RC (serotype 9), using a standard calcium phosphate method. Transfected cells were collected after three days and suspended in Hank's Balanced Salt Solution (Merck). The AAV-containing cell lysate was treated with 250 U/ml benzonase at 37 °C for 30 min without adding $MgCl_2$, and then centrifuged three times at 17,800×g for 10 min at 4°C with the supernatant after each centrifugation used for the next centrifugation. The final supernatant was then aliquoted and stored at −80°C.

Surveyor nuclease cleavage assay

To examine the off-target effect of our saCas9-*Drd1a*-gRNA, we performed Surveyor nuclease cleavage assay as previously described (*44*). Briefly, the *Drd1a*- or empty pX601 plasmid was transfected into Neuro2A cells in a 24-well plate using Lipofectamine LTX (Life Technologies). After 72 h post-transfection, genomic DNA was isolated using a DNeasy Blood & Tissue kit (QIAGEN). *Drd1a* loci were then amplified from the purified genomic DNA with PCR. PCR products were denatured, digested at 42°C for 30 min with a Surveyor Mutation Detection kit (Transgenomic), and analyzed by electrophoresis in 3% agarose gel stained with ethidium bromide. The gel images were obtained with a ChemiDoc XRS system (Bio-Rad) and analyzed by Image Lab software (Bio-Rad).

Animal preparation and surgery

Mice were anesthetized with isoflurane (3.0–3.5% for induction, 1.0–1.5% for maintenance) and head-fixed on a stereotactic device using ear bars or a nose clamp. Body temperature was maintained at ~37°C by a controlled heating pad. An ocular ointment was applied over the eyes to prevent drying. The scalp was cut open to expose the skull. For *in vivo* genome editing (Fig. 4, C and D), AAV harboring *Drd1a*-targeting guide RNA or control guide RNA was bilaterally injected into four sites targeting the NAc (AP: 1 mm, ML: ±1.2 mm, from Bregma, depth: 3.8 mm; and AP: 1.5 mm, ML: ±1.2 mm, from Bregma, depth: 4.0 mm) through small craniotomies (diameter, <~0.5 mm). The injection volume was 500 nl per site. For the experiment with optogenetic axonal stimulation (Fig. 4, E and F), AAV-Ef1a-DIO-bReaChES-TS-eYFP (titer: 6.0×10^{13} copies/ml) or AAV-CMV-DIO-hrGFP (titer: 6.0×10^{12} copies/ml) was injected bilaterally into the VTA (AP: −3.0 mm, ML: ±0.5 mm, from Bregma, depth: 4.2 mm) of DAT-IRES-Cre mice. The injection volume was 200 nl per site. For the experiment with optogenetic stimulation of the SNc-DA neurons (fig. S4), AAV9-Ef1a-DIO-hChR2(E123T/T159C)-EYFP (Addgene #35509, obtained from Addgene; the original titer: 2.2×10^{13} copies/ml, diluted to 1/10) or AAV9- Ef1a-DIO-EYFP (Addgene #27056, obtained from Addgene; the original titer: 2.7×10^{13} copies/ml, diluted to 1/10) was injected into the left SNc (AP: -3.1 mm, ML: 1.2 mm, from Bregma, depth: 4.1 mm) of DAT-IRES-Cre mice. The injection volume was 200 nl. For optogenetic stimulation of wM1, AAV-CaMKIIa-hChR(E123T/T159C)-mCherry (Addgene #35512, obtained from Addgene; the original titer, 3.0×10^{13} copies/ml, diluted to 1/10) was injected unilaterally into the wM1 (AP: 1.0 mm, ML: 1.0 mm, from Bregma, depth: 0.85 mm and 0.35 mm) of wild-type C57BL6/J mice. The injection volume was 200 nl per site. With the scalp sutured, the mice were returned to their home cages for at least three weeks after the AAV injection before behavioral experiments.

Prior to behavioral experiments, mice were implanted with a light-weight metal head-holder (*39*). For optogenetic stimulation, pharmacological perturbation, or silicone probe recordings in left wM1, a chamber was made on the left hemisphere by building a wall with dental cement, and a thin layer of glue was applied over the exposed skull. For optogenetic stimulation of deep brain regions, we used an optical fiber (0.4 mm diameter) attached to a stainless steel ferrule (CFM14L05, Thorlabs) which was implanted over the left NAc (AP: 1.25 mm, ML: 1.5 mm, from Bregma, depth: 3.8 mm) or the left VTA (AP: −3.0 or −3.3 mm, ML: ±0.3 or 0.5 mm, from Bregma, depth: 4.0 mm). The optical fiber cannula was permanently cemented to the skull. For optogenetic stimulation of wM1, we made a small craniotomy over the left wM1 and placed the optical fiber over the craniotomy.

Behavioral tasks

Whisker detection task

To examine the orofacial movements of mice performing a whisker detection task (*31*), we analyzed the data obtained from the mice used for recording in our previous paper (*39*). The procedure of the whisker detection task was previously described (*39*). All whiskers except for the right C2 whisker were trimmed before experiments. We applied a brief (1 ms) magnetic pulse to elicit a vertical deflection of the right C2 whisker transmitted by small metal particles glued on the whisker. The mice under head-fixation were trained to learn the availability of water reward within a 1-s window after the whisker stimulation. The whisker was filmed at 500 Hz with a high-speed camera. The behavioral signals from the lick sensor together with TTL signals to control the water valve and the electromagnetic coil were recorded through an NI board. In some recordings, it was impossible to extract the whisker position due to the metal particles covering the basal part of the whisker. Therefore, we only included the data

where the basal part of the whisker was partially exposed. Novice mice had no prior task experience and showed a low hit rate (31.1 ± 4.2%, n = 6 mice). Expert mice analyzed in this study were trained for the task in 8–17 daily sessions before the recording day and exhibited a high hit rate (79.2 ± 3.6%, n = 6 mice).

Auditory Go/No-Go task

At least three days after implantation of the metal head holder, adult male C57Bl6/J mice started to be water-restricted. The mice were adapted to head restraint on the experimental setup through initial training to freely lick the water spout for receiving a water reward (3–5 sessions, one session per day). The mice were then taught, through daily training sessions, to associate a pure tone (2 s) with water availability within a 1-s window after the offset of tone presentation. Trials were started with a 3 kHz tone ("Go" cue) or a 15 kHz tone ("No-Go" cue) following random inter-trial intervals ranging from 3 to 9 s. In some experiments, the "Go" tone and "No-Go" tone were swapped. If the mice licked in the 2 s preceding the time when the trial was supposed to occur, then the trial was aborted, and a subsequent trial started. Lick was detected with a piezo sensor attached to the water spout. After each training session, 1.0–1.5 g of wet food pellet was given to the mouse to keep its body weight above 80% of the initial value. Behavioral control was carried out using a custom-written program on Python interfaced through Arduino Uno. All whiskers except for the right C2 whisker were trimmed before experiments. The whisker was filmed at 200 Hz with a high-speed camera. Behavioral data were acquired using an NI board. Novice mice were defined by poor performance (daily d' < 1.0). These mice were typically on the first day of task training and showed an average hit rate of 33.7 ± 5.5% (n = 9 mice). Expert mice were defined as those keeping a high performance (daily d'> 2.5) for five successive days. These mice showed an average hit rate

of 94.1 ± 1.4% (n = 7 mice). One mouse underwent a reversal-learning: after the mouse learned the task with a 3-kHz tone as a Go-cue, then we swapped the Go and No-Go tones. The mouse successfully learned the swapped association, and the data were pooled into the dataset as a different experiment from the initial learning.

Optogenetics

Optogenetic stimulation in head-fixed mice

All the behavioral experiments using optogenetic stimulation followed the habituation of mice to head-fixation for three days. The duration of habituation was ~15 min on the first day, ~30 min on the second day, and ~60 min on the third day. All whiskers were trimmed except the left C2 whiskers or the left and right C2 whiskers before the experiments. For optogenetic stimulation of DA neurons, blue LED (470 nm; M470F3, Thorlabs) light was applied over the VTA or SNc of DAT-ChR2 mice or control Ai32 mice through the implanted optic fiber. For stimulating bReaChES/hrGFP-expressing DA axons in the NAc, green LED (530 nm; M530F2, Thorlabs) light was applied over the NAc through the implanted optic fiber. For stimulating ChR2-expressng neurons in wM1, the blue LED light was applied through the craniotomy made over the left M1. 20 pulses of 5-ms light stimuli were applied at 20 Hz unless otherwise noted. The light power at the fiber tip was 15.8 mW for the blue light and 6.6 mW for the green light unless otherwise noted. The frontal mouse face, including its nose and whisker(s), was filmed at 500 Hz from above with a high-speed camera. Through immunostaining (see below), we routinely checked the location of implanted optical fiber and discarded data when the fiber tip was found to be more than 0.5 mm away from the target or inserted too deep damaging the target brain structure.

Sound-oDAS pairing conditioning

For the Pavlovian sound-oDAS conditioning, we used the mice that experienced oDAS. We habituated the mice to a 15-kHz tone presentation (5 s) by being exposed to the tone stimuli 20 times with random intervals of 60–120 s under head fixation on the day before starting the conditioning. For the conditioning, we presented to the mice the 15-kHz sound cue (5 s) paired with oDAS (5 ms, 20 times at 20 Hz) at the last 1 s of the cue. The inter-trial interval was set randomly for each trial to be from 180–240 s. A custom-written program on Python interfaced through Arduino Uno controlled the timings of sound cue presentation and light stimulation, which were synchronized with filming the mouse's frontal face from above. The mice experienced ~20 paired stimuli in each daily session.

Pharmacological perturbation

To examine the effect of a D1R antagonist on orofacial movements, we first calculated the injection volume of SCH23390 (0.3 mg/kg) or raclopride (3 mg/kg) for each experimental mouse and injected saline of the calculated volume intraperitoneally into the mouse. The behavioral recording was started 15 min after injection. After the recording session with saline injection, the mice were subjected to an IP injection of the D1R/D2R antagonists, and the behavioral recording was resumed 15 min after injection.

To examine the effect of wM1 inactivation on orofacial experiments, we first made a small craniotomy over wM1 of DAT-ChR2 mice under anesthesia. After recovery from anesthesia, the mouse was head-fixed to the experimental setup, and the behavior was recorded. Subsequently, 100 nl of Ringer's solution with or without muscimol (5 mM) was injected into at 900, 700, 500, 300, and 100 μm each below the surface using a glass pipette inserted through the craniotomy. A small volume of Chicago Sky Blue was mixed in the

muscimol solution. The whole injection period was 20–30 min. The behavioral tests were resumed after the injection pipette was slowly withdrawn.

Immunostaining

After behavioral and electrophysiological experiments, we routinely performed transcardial perfusion of the mice with 4% paraformaldehyde (PFA). The brain was removed and incubated with 4% PFA solution overnight for post-fixation. The fixed brain was then kept in phosphate buffer (PB) until further processing. The fixed brain was sectioned into coronal slices on a vibratome (section thickness: 100 μm). For immunostaining of brain slices, the slices were washed three times with a blocking buffer containing 1% bovine serum albumin and 0.25% Triton-X in phosphate buffer saline (PBS) and then incubated with primary antibodies (anti-tyrosine hydroxylase, rabbit polyclonal, 1:1000, Merck Millipore; anti-D1R, guinea pig polyclonal, 1:200, Frontier Institute; anti-GFP, mouse monoclonal, 1:1000, Fujifilm Wako Chemicals) in the blocking buffer overnight at 4 °C. The slices were then washed three times with the blocking buffer and then incubated with secondary antibodies (CF594-conjugated donkey anti-rabbit IgG, 1:1000, Biotium; CF488A-conjugated goat anti-mouse IgG, 1:1000, Biotium; CF594-conjugated donkey anti-guinea pig IgG, 1:1000, Biotium) in the blocking buffer for 1–2 h at room temperature (RT). Cellular nuclei were stained by incubation for 10–15 min with DAPI (2 μM in PB) at RT. The stained samples were mounted using DABCO and observed under a fluorescence microscope (BZ-9000, Keyence). Images were saved using BZ-X Viewer (Keyence).

Electrophysiology

A small craniotomy was made over the left wM1 (1 mm anterior, 1 mm lateral from Bregma). Extracellular spikes were recorded in head-fixed mice using a silicon probe (A1x32-Poly2-10mm50s-177, NeuroNexus) with 32 recording sites along a single shank, covering 775 mm of the cortical depth. The probe was lowered gradually until the tip was positioned at a depth of 1.0–1.1 mm under the wM1 pial surface. The craniotomy site was then covered with 1.5% agarose dissolved in Ringer's solution. Neural data were filtered between 0.5 Hz and 7.5 kHz, amplified using a digital head-stage (RHD2132, Intan Technologies), and digitized with a sampling frequency of 30 kHz. The digitized neural signal was transferred to an acquisition board (Open Ephys) and stored on an internal HDD of the host PC for offline analysis. The TTL pulses for the sound and light stimulation were also recorded through the Open Ephys acquisition board. Spiking activity on each probe was detected and sorted into different clusters using Kilosort (https://github.com/cortex-lab/KiloSort). After an automated clustering step, clusters were manually sorted and refined using Phy (https://github.com/cortex-lab/phy). Only well-isolated single units (174 units) were included in the dataset.

Data analysis

Motion energy analysis

Mouse facial movements were quantified by analyzing the side-view (Fig. 2B) and top-view (Fig. 2C) movies. Motion energy was computed as the absolute value of the difference of consecutive frames obtained during oDAS (for 1 s) and at the baseline (0-1 s before the stimulus onset). The motion energy heat-map is shown as the difference between motion energy during oDAS and at the baseline in each pixel. For quantification (Fig. 2B), we set polygonal regions of interest around the ear or orofacial area and calculated the mean change in motion energy evoked by the oDAS by comparing values during oDAS and at baseline.

Analysis of whisker movements

Movements of the right C2 whisker were quantified offline with ImageJ using an open source macro (https://github.com/tarokiritani/WhiskerTracking) and the data were analyzed with Igor Pro or MATLAB. The total whisker movements (ΣWM) were calculated as the cumulative whisker movements during oDAS (Fig. 2, 4, 6, and fig S2, S3, S4, S5, S6, S7, and S10) or at 0–1 s after the reward time window for the data in the reward-based learning tasks (Fig. 1). Data with the prominent whisking starting during the 1-s period before the onset of oDAS (Fig. 2, 4, 6, and fig S2, S3, S4, S5, S6, S7, and S10) or the conditioning stimulus (Fig. 3, 5, 7 and fig S3, S5, S6, S8, S10, and S11) were excluded from the analysis. When the ΣWM during oDAS exceeded 90 deg, the data were defined as epochs with whisking induced (WM+). A cue-locked whisker protraction was defined as a whisker protraction of more than 5 deg above baseline within 0.5 s after the onset of cue presentation. The onset time of whisker movement or whisker protraction was taken as the time at which the whisker angle exceeded 1 deg above baseline, among these epochs with whisker movement or cue-locked whisker protraction.

Analysis of nose movements

We quantified nose movement using the markerless video tracking software, DeepLabCut (*40*). As illustrated in Fig. 2E, we manually annotated the five points of the top-view nose (left and right anterior/posterior edges and nose tip) using 60–340 frames per movie to train a deep neural network. An estimated position with a low likelihood (<0.8) was omitted and replaced with a pixel value obtained using linear interpolation of neighboring values (*58*). The nose area was the area of the pentagon formed by the estimated five points. The nose length

in the anterior-posterior axis was taken as the distance between the nose tip and the middle point of the posterior nose edges. The lateral movement of the nose tip was the displacement of the horizontal coordinate of the nose tip quantified as the percentage with the average anterior-posterior nose length taken as 100%. The onset of lateral nose tip movement was defined as the time point where the trace exceeded three times of standard deviation of the baseline (0–1 s before the stimulus/cue onset). The latency of nose movement was defined as the time difference between the stimulus/cue onset and the onset of lateral nose tip movement. The data with whisking at the pre-stimulus period (1 s) were excluded from the analysis of nose movement.

Machine learning for classifying trial categories based on whisker movements

For decoding trial categories (“Hit” or “CR”) of the auditory Go/No-Go task using the whisker time plot, we selected “Hit” and “CR” trials from the dataset, excluding “Miss” and “FA (false alarm)” trials. The data for each trial was filtered by a band-pass filter (4–20 Hz) and then transformed into a power spectrogram by short-term Fourier transformation with 200-ms or 100-ms bins. We extracted the power spectrogram at 4–20 Hz and then linearly normalized the spectrogram so that the sum of powers equals one in each time bin. We made power spectrum matrices with 240 dimensions (24 frequency domains x 10 time domains) for the data at the cue period (2 s) or at 0–1 s after the reward time window (after RA). Among the data from seven expert mice, we pooled the data from six mice as training data, excluding the one from one mouse as test data, and applied the principal component (PC) analysis on MATLAB to make a PC space with two dimensions. We used this PC space to obtain the first and second PC scores for each trial of the test data and plotted them (Fig. 1H). We constructed a logistic regression model using the PC plot obtained from training data, which

outputs a likelihood (minimum: 0, maximum: 1) of being “Hit” for each trial of the test data. The trials with a likelihood of more than 0.5 were predicted as “Hit” trials, and otherwise, the trials were predicted as “CR” trials. The decoding accuracy is a fraction of the number of correct predictions over the total trial number of the test data. We repeated the same procedure for the other six mice (a process called leave-one-subject-out cross-validation).

Classification of single units

Single units recorded with the silicone probe were classified as fast-spiking (FS) putative interneurons or regular-spiking (RS) putative pyramidal cells based on their trough-to-peak time of average spike waveform. Single units with a trough-to-peak time < 0.35 ms were classified as FS cells, and units with a trough-to-peak time > 0.35 ms were classified as RS cells.

Analysis of the correlation between spike rates and whisker behavior

We classified wM1 cells based on their correlation with whisker behavior during the sound-oDAS pairing tests. We first categorized the trials into four categories (Fig. 7A): “RE+RA trials” are trials with both cue-locked whisker protraction and oDAS-aligned whisker movements; “RE trials” are trials with cue-locked whisker protraction but without oDAS-aligned whisker movements; “RA trials” are trials with oDAS-aligned whisker movements but without cue-locked whisker protraction; and “No reward-related WMs trials” are trials with neither cue-locked whisker protraction nor oDAS-aligned whisker movements. We used different trial categories: “Cue-WP+ trials” are RE+RA and RE trials; “Cue-WP- trials” are RA and No reward-related WMs trials; “oDAS-WM+ trials” are RE+RA and RA trials; and “oDAS-WM- trials” are RE and No reward-related WMs trials. We defined the cellular categories as follows:

“RE+RA cells” showed a significantly higher firing rate at the cue onset (1 s) in Cue-WP+ trials than in Cue-WP- trials, and also showed a significantly higher firing rate during oDAS in oDAS-WM+ trials than in oDAS-WM- trials; “RE cells” showed a significantly higher firing rate at the cue onset (1 s) in Cue-WP+ trials than in Cue-WP- trials, and exhibit similar firing during oDAS in oDAS-WM+ and oDAS-WM- trials; “RA cells” showed a significantly higher firing rate during oDAS in oDAS-WM+ trials than in oDAS-WM- trials, and exhibit similar firing at the cue onset (1 s) in Cue-WP+ and Cue-WP- trials. In Fig. 7E, we plotted “RE correlation” as the Pearson correlation coefficients between spike rates and the maximal WP amplitudes during 1 s at the cue onset and “RA correlation” as the Pearson correlation coefficients between spike rates and the variances of the whisker position during oDAS.

Statistics

All values are expressed as mean ± SEM except for the box plots in the figures. Statistical tests were performed using GraphPad Prism. The normality of data distribution was routinely tested. Analyses of two sample comparisons were performed using unpaired or paired *t* tests when each sample was normally distributed, or Wilcoxon signed rank test (paired) or Mann-Whitney *U* test (unpaired) when at least one of the samples in every two-sample comparison was not normally distributed. Tests for two-sample comparison were two-sided. Statistical analyses for multiple comparisons were carried out using one- or two-way ANOVA followed by Bonferroni’s multiple comparison tests or Dunnett’s multiple comparison tests vs. the control, unless otherwise noted. For correlation analysis, Pearson’s correlation coefficient (*r*) for normally distributed sets of data or Spearman’s rank correlation coefficient (rho) for randomly distributed data was calculated.

REFERENCES

1. C. R. Darwin, *The expression of the emotions in man and animals.* (London, Murray, 1872).
2. J. A. R. A. M. Van Hooff, "The facial displays of the catarrhine monkeys and apes." in *Primate ethology,* D. Morris, Ed. (1967), pp. 7-68.
3. M. W. Fox, The anatomy of aggression and its ritualization in canidae: a developmental and comparative study. *Behaviour* **35**, 242-258 (1969).
4. M. B. H. Schilder, J. A. R. A. M. van Hooff, C. J. van Geer-Plesman, J. B. Wensing, A quantitative analysis of facial expression in the Plains Zebra. *Zeitschrift für Tierpsychologie* **66**, 11-32 (1984).
5. D. J. Langford, A. L. Bailey, M. L. Chanda, S. E. Clarke, T. E. Drummond, S. Echols, S. Glick, J. Ingrao, T. Klassen-Ross, M. L. Lacroix-Fralish, L. Matsumiya, R. E. Sorge, S. G. Sotocinal, J. M. Tabaka, D. Wong, A. M. van den Maagdenberg, M. D. Ferrari, K. D. Craig, J. S. Mogil, Coding of facial expressions of pain in the laboratory mouse. *Nat Methods* **7**, 447-449 (2010).
6. E. B. Defensor, M. J. Corley, R. J. Blanchard, D. C. Blanchard, Facial expressions of mice in aggressive and fearful contexts. *Physiol Behav* **107**, 680-685 (2012).
7. K. Finlayson, J. F. Lampe, S. Hintze, H. Wurbel, L. Melotti, Facial indicators of positive emotions in rats. *PLoS One* **11**, e0166446 (2016).
8. N. Dolensek, D. A. Gehrlach, A. S. Klein, N. Gogolla, Facial expressions of emotion states and their neuronal correlates in mice. *Science* **368**, 89-94 (2020).
9. S. Sachidhanandam, V. Sreenivasan, A. Kyriakatos, Y. Kremer, C. C. H. Petersen, Membrane potential correlates of sensory perception in mouse barrel cortex. *Nat Neurosci* **16**, 1671-1677 (2013).
10. S. Musall, M. T. Kaufman, A. L. Juavinett, S. Gluf, A. K. Churchland, Single-trial neural dynamics are dominated by richly varied movements. *Nat Neurosci* **22**, 1677-1686 (2019).
11. S. E. Dominiak, M. A. Nashaat, K. Sehara, H. Oraby, M. E. Larkum, R. N. S. Sachdev, Whisking asymmetry signals motor preparation and the behavioral state of mice. *J Neurosci* **39**, 9818-9830 (2019).

12. D. B. Salkoff, E. Zagha, E. McCarthy, D. A. McCormick, Movement and performance explain widespread cortical activity in a visual detection task. *Cereb Cortex* **30**, 421-437 (2020).

13. V. Esmaeili, K. Tamura, S. P. Muscinelli, A. Modirshanechi, M. Boscaglia, A. B. Lee, A. Oryshchuk, G. Foustoukos, Y. Liu, S. Crochet, W. Gerstner, C. C. H. Petersen, Rapid suppression and sustained activation of distinct cortical regions for a delayed sensory-triggered motor response. *Neuron* **109**, 2183-2201 (2021).

14. M. Deschênes, J. Moore, D. Kleinfeld, Sniffing and whisking in rodents. *Curr Opin Neurobiol* **22**, 243-250 (2012).

15. H. Welzl, J. Bureš, Lick-synchronized breathing in rats. *Physiol Behav* **18**, 751-753 (1977).

16. J. D. Moore, M. Deschenes, T. Furuta, D. Huber, M. C. Smear, M. Demers, D. Kleinfeld, Hierarchy of orofacial rhythms revealed through whisking and breathing. *Nature* **497**, 205-210 (2013).

17. A. Kurnikova, J. D. Moore, S. M. Liao, M. Deschenes, D. Kleinfeld, Coordination of orofacial motor actions into exploratory behavior by rat. *Curr Biol* **27**, 688-696 (2017).

18. W. Schultz, P. Dayan, P. R. Montague, A neural substrate of prediction and reward. *Science* **275**, 1593-1599 (1997).

19. K. C. Berridge, T. E. Robinson, What is the role of dopamine in reward: hedonic impact, reward learning, or incentive salience? *Brain Res Brain Res Rev* **28**, 309-369 (1998).

20. K. C. Berridge, M. L. Kringelbach, Pleasure systems in the brain. *Neuron* **86**, 646-664 (2015).

21. H. C. Tsai, F. Zhang, A. Adamantidis, G. D. Stuber, A. Bonci, L. de Lecea, K. Deisseroth, Phasic firing in dopaminergic neurons is sufficient for behavioral conditioning. *Science* **324**, 1080-1084 (2009).

22. A. R. Adamantidis, H. C. Tsai, B. Boutrel, F. Zhang, G. D. Stuber, E. A. Budygin, C. Tourino, A. Bonci, K. Deisseroth, L. de Lecea, Optogenetic interrogation of dopaminergic modulation of the multiple phases of reward-seeking behavior. *J Neurosci* **31**, 10829-10835 (2011).

23. V. Pascoli, A. Hiver, R. Van Zessen, M. Loureiro, R. Achargui, M. Harada, J. Flakowski, C. Lüscher, Stochastic synaptic plasticity underlying compulsion in a model of addiction. *Nature* **564**, 366-371 (2018).

24. C. P. Burgess, A. Lak, N. A. Steinmetz, P. Zatka-Haas, C. Bai Reddy, E. A. K. Jacobs, J. F. Linden, J. J. Paton, A. Ranson, S. Schroder, S. Soares, M. J. Wells, L. E. Wool, K. D. Harris, M. Carandini, High-yield methods for accurate two-alternative visual psychophysics in head-fixed mice. *Cell Rep* **20**, 2513-2524 (2017).

25. J. Y. Cohen, S. Haesler, L. Vong, B. B. Lowell, N. Uchida, Neuron-type-specific signals for reward and punishment in the ventral tegmental area. *Nature* **482**, 85-88 (2012).

26. J. Tian, N. Uchida, Habenula lesions reveal that multiple mechanisms underlie dopamine prediction errors. *Neuron* **87**, 1304-1316 (2015).

27. C. K. Starkweather, B. M. Babayan, N. Uchida, S. J. Gershman, Dopamine reward prediction errors reflect hidden-state inference across time. *Nat Neurosci* **20**, 581-589 (2017).

28. M. Brecht, M. Schneider, B. Sakmann, T. W. Margrie, Whisker movements evoked by stimulation of single pyramidal cells in rat motor cortex. *Nature* **427**, 704-710 (2004).

29. F. Matyas, V. Sreenivasan, F. Marbach, C. Wacongne, B. Barsy, C. Mateo, R. Aronoff, C. C. Petersen, Motor control by sensory cortex. *Science* **330**, 1240-1243 (2010).

30. V. Sreenivasan, K. Karmakar, F. M. Rijli, C. C. Petersen, Parallel pathways from motor and somatosensory cortex for controlling whisker movements in mice. *Eur J Neurosci* **41**, 354-367 (2015).

31. V. Sreenivasan, V. Esmaeili, T. Kiritani, K. Galan, S. Crochet, C. C. H. Petersen, Movement initiation signals in mouse whisker motor cortex. *Neuron* **92**, 1368-1382 (2016).

32. N. Mercer Lindsay, P. M. Knutsen, A. F. Lozada, D. Gibbs, H. J. Karten, D. Kleinfeld, Orofacial movements involve parallel corticobulbar projections from motor cortex to trigeminal premotor nuclei. *Neuron* **104**, 765-780 (2019).

33. D. N. Hill, J. C. Curtis, J. D. Moore, D. Kleinfeld, Primary motor cortex reports efferent control of vibrissa motion on multiple timescales. *Neuron* **72**, 344-356 (2011).

34. W. A. Friedman, H. P. Zeigler, A. Keller, Vibrissae motor cortex unit activity during whisking. *J Neurophysiol* **107**, 551-563 (2012).

35. T. V. Gerdjikov, F. Haiss, O. E. Rodriguez-Sierra, C. Schwarz, Rhythmic whisking area (RW) in rat primary motor cortex: an internal monitor of movement-related signals? *J Neurosci* **33**, 14193-14204 (2013).

36. F. Caruana, A. Jezzini, B. Sbriscia-Fioretti, G. Rizzolatti, V. Gallese, Emotional and

social behaviors elicited by electrical stimulation of the insula in the macaque monkey. *Curr Biol* **21**, 195-199 (2011).

37. H. J. Grill, R. Norgren, Chronically decerebrate rats demonstrate satiation but not bait shyness. *Science* **201**, 267-269 (1978).

38. H. J. Grill, R. Norgren, The taste reactivity test. II. Mimetic responses to gustatory stimuli in chronic thalamic and chronic decerebrate rats. *Brain Res* **143**, 281-297 (1978).

39. T. Yamashita, C. C, H. Petersen, Target-specific membrane potential dynamics of neocortical projection neurons during goal-directed behavior. *eLife* **5**, e15798 (2016).

40. A. Mathis, P. Mamidanna, K. M. Cury, T. Abe, V. N. Murthy, M. W. Mathis, M. Bethge, DeepLabCut: markerless pose estimation of user-defined body parts with deep learning. *Nat Neurosci* **21**, 1281-1289 (2018).

41. P. D. Dodson, J. K. Dreyer, K. A. Jennings, E. C. Syed, R. Wade-Martins, S. J. Cragg, J. P. Bolam, P. J. Magill, Representation of spontaneous movement by dopaminergic neurons is cell-type selective and disrupted in parkinsonism. *Proc Natl Acad Sci U S A* **113**, E2180-E2188 (2016).

42. M. W. Howe, D. A. Dombeck, Rapid signalling in distinct dopaminergic axons during locomotion and reward. *Nature* **535**, 505-510 (2016).

43. L. A. Gunaydin, L. Grosenick, J. C. Finkelstein, I. V. Kauvar, L. E. Fenno, A. Adhikari, S. Lammel, J. J. Mirzabekov, R. D. Airan, K. A. Zalocusky, K. M. Tye, P. Anikeeva, R. C. Malenka, K. Deisseroth, Natural neural projection dynamics underlying social behavior. *Cell* **157**, 1535-1551 (2014).

44. W. Cui, T. Aida, H. Ito, K. Kobayashi, Y. Wada, S. Kato, T. Nakano, M. Zhu, K. Isa, K. Kobayashi, T. Isa, K. Tanaka, H. Aizawa, Dopaminergic signaling in the nucleus accumbens modulates stress-coping strategies during inescapable stress. *J Neurosci* **40**, 7241-7254 (2020).

45. C. Stringer, M. Pachitariu, N. Steinmetz, C. B. Reddy, M. Carandini, K. D. Harris, Spontaneous behaviors drive multidimensional, brainwide activity. *Science* **364**, eaav7893 (2019).

46. D. Bindra, J. F. Campbell, Motivational effects of rewarding intracranial stimulation. *Nature* **215**, 375-376 (1967).

47. S. Clarke, J. A. Trowill, Sniffing and motivated behavior in the rat. *Physiol Behav* **6**, 49-52 (1971).

48. A. Kepecs, N. Uchida, Z. F. Mainen, The sniff as a unit of olfactory processing. *Chem Senses* **31**, 167-179 (2006).

49. B. T. Saunders, J. M. Richard, E. B. Margolis, P. H. Janak, Dopamine neurons create Pavlovian conditioned stimuli with circuit-defined motivational properties. *Nat Neurosci* **21**, 1072-1083 (2018).

50. W. I. Welker, Analysis of sniffing of the albino rat. *Behaviour* **22**, 223-244 (1964).

51. H. M. Bayer, P. W. Glimcher, Midbrain dopamine neurons encode a quantitative reward prediction error signal. *Neuron* **47**, 129-141 (2005).

52. C. C. H. Petersen, Cortical control of whisker movement. *Annu Rev Neurosci* **37**, 183-203 (2014).

53. L. E. McElvain, B. Friedman, H. J. Karten, K. Svoboda, F. Wang, M. Deschenes, D. Kleinfeld, Circuits in the rodent brainstem that control whisking in concert with other orofacial motor actions. *Neuroscience* **368**, 152-170 (2018).

54. T. Patriarchi, J. R. Cho, K. Merten, M. W. Howe, A. Marley, W. H. Xiong, R. W. Folk, G. J. Broussard, R. Liang, M. J. Jang, H. Zhong, D. Dombeck, M. von Zastrow, A. Nimmerjahn, V. Gradinaru, J. T. Williams, L. Tian, Ultrafast neuronal imaging of dopamine dynamics with designed genetically encoded sensors. *Science* **360**, eaat4422 (2018).

55. T. M. Otchy, S. B. Wolff, J. Y. Rhee, C. Pehlevan, R. Kawai, A. Kempf, S. M. Gobes, B. P. Olveczky, Acute off-target effects of neural circuit manipulations. *Nature* **528**, 358-363 (2015).

56. Y. K. Hong, C. O. Lacefield, C. C. Rodgers, R. M. Bruno, Sensation, movement and learning in the absence of barrel cortex. *Nature* **561**, 542-546 (2018).

57. L. Madisen, T. Mao, H. Koch, J. M. Zhuo, A. Berenyi, S. Fujisawa, Y. W. Hsu, A. J. Garcia, 3rd, X. Gu, S. Zanella, J. Kidney, H. Gu, Y. Mao, B. M. Hooks, E. S. Boyden, G. Buzsaki, J. M. Ramirez, A. R. Jones, K. Svoboda, X. Han, E. E. Turner, H. Zeng, A toolbox of Cre-dependent optogenetic transgenic mice for light-induced activation and silencing. *Nat Neurosci* **15**, 793-802 (2012).

58. T. Matsubara, T. Yanagida, N. Kawaguchi, T. Nakano, J. Yoshimoto, M. Sezaki, H. Takizawa, S. P. Tsunoda, S. I. Horigane, S. Ueda, S. Takemoto-Kimura, H. Kandori, A. Yamanaka, T. Yamashita, Remote control of neural function by X-ray-induced scintillation. *Nat Commun* **12**, 4478 (2021).

ACKNOWLEDGEMENTS

We thank Dr. H. Kasai for providing DAT-IRES-Cre mice; Dr. K. Ono for providing Ai32 mice; Dr. K. Deisseroth for providing bReaChES plasmid; Drs. T. Hikida, Y. Ohmura and J. Dijkstra for discussion; J. Ozaki for collaboration at the early phase of the study; N. Fukatsu for helping with nose analysis; E. Charrière, S. Tsukamoto, A. Kambara, M. Jin, E. Imoto for technical assistance.

Funding: This work was supported by JSPS KAKENHI grants (17H05744, 18K19496, 21H00215) to TY; The Naito Foundation to TY; Takeda Science Foundation to TY; JNNS30 Commemorative Research Grant to JY.

Author contributions: WL, TN, KM, JY, and TY designed the study. WL, KM, MK, TM, and TY performed experiments and analyzed data. TN and JY developed machine learning algorithms and analyzed data. TD developed Matlab codes for motion energy analysis. YM and AY provided AAVs for in vivo genome editing and contributed to interpreting the results. HI and HA provided plasmids for in vivo genome editing, performed Surveyor nuclease cleavage assays and analyzed the data. TY and CCHP contributed to data collection related to the whisker detection task. WL and TY drafted and wrote the manuscript with inputs from other co-authors.

Competing interests: The authors declare that they have no competing interests.

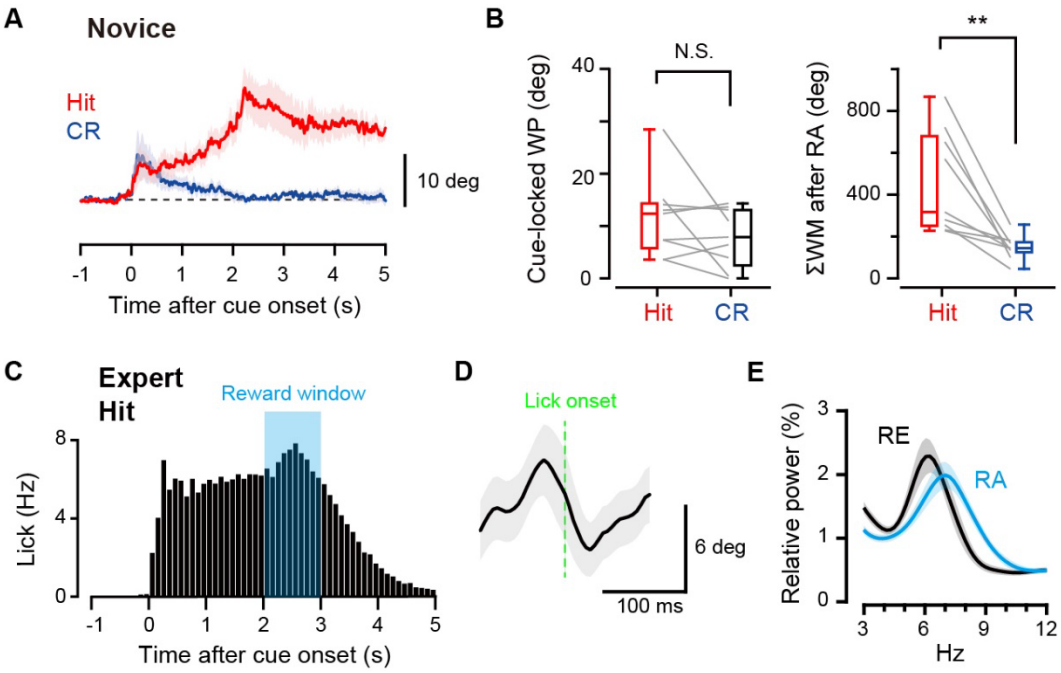

Fig. S1. Additional analyses of orofacial behaviors during the auditory Go/No-Go task. (**A**) Grand averages of whisker movements in hit (red) and CR (blue) trials from 9 novice mice. (**B**) Data for each mouse (thin lines) and box plots for the amplitudes of the cue-locked whisker protraction (WP) (left) and total whisker movement (ΣWM) 0-1s after reward window (right), in hit (H) and miss (M) trials during the auditory Go/No-Go task, obtained from novice mice. (**C**) Average lick PSTH during the auditory Go/No-Go task obtained from 7 expert mice. Light blue shadow: reward time window. (**D**) Lick-triggered average whisker trace at the cue period obtained from 7 expert mice. (**E**) Relative power spectra of whisker movements during the cue period (RE) and the reward time window (RA) obtained from 7 expert mice. Thick line and shadows in (D) and (E) indicate mean ± SEM. **$p < 0.01$, N.S., not significant, paired *t* test.

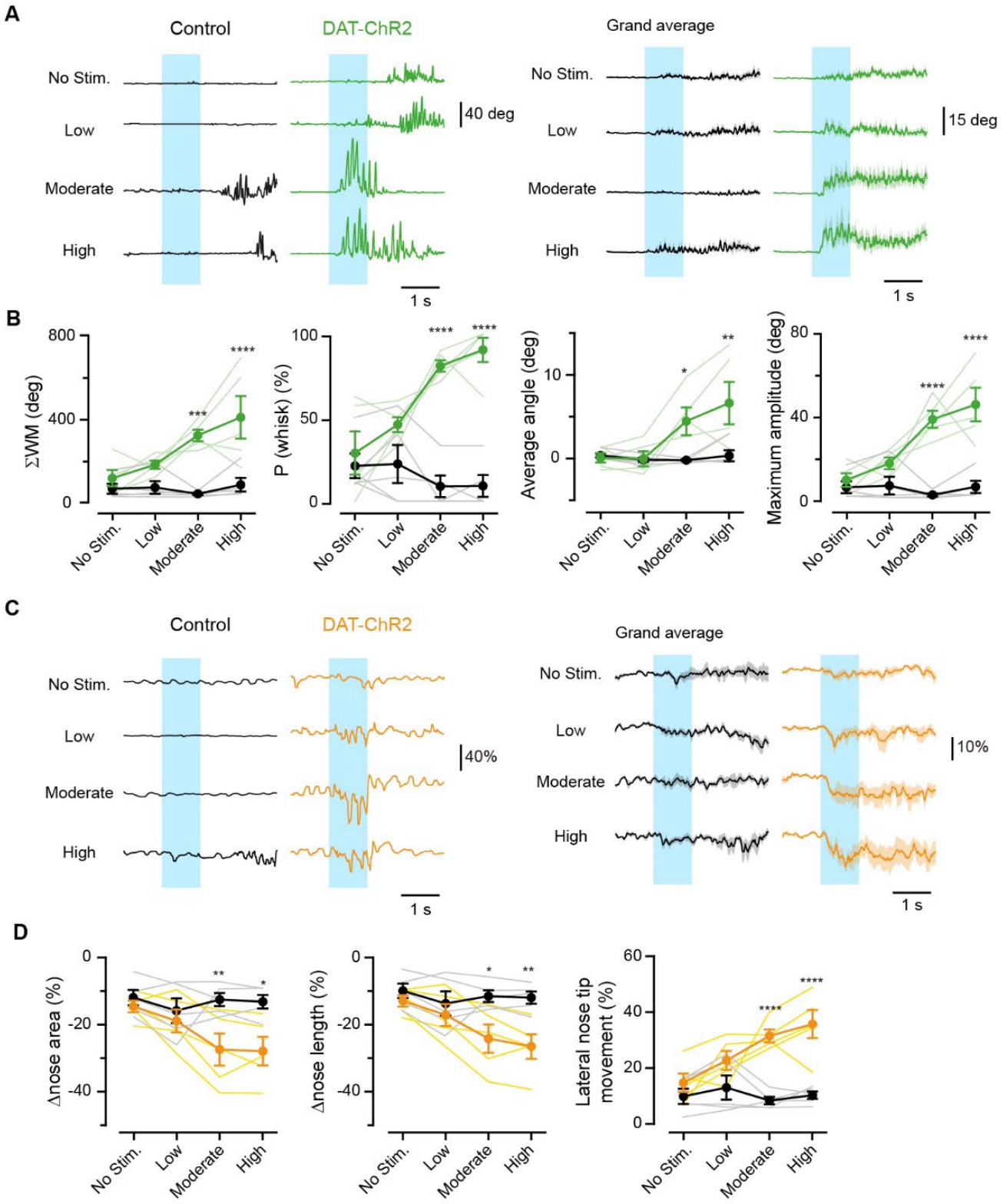

Fig. S2. oDAS-Induced orofacial movements with different stimulus intensities. (**A**) Left, example traces of the whisker position upon oDAS (light blue shadow) with different photo-stimulus

intensities, obtained from a control (black) and DAT-ChR2 (green) mouse. The light intensity at the fiber tip was 3.0 mW (low), 7.6 mW (moderate), or 15.8 mW (high). Right, grand average of the whisker position upon oDAS (n = 5 mice for each). (**B**) ΣWM, P(whisk), and average and maximal amplitude of WMs during oDAS. (**C**) Same as (A) but for traces of the top-view nose area from control (black) or DAT-ChR2 (orange) mice. (**D**) Quantifications for the changes in nose area (left), nose length in the anterior-posterior axis (middle), and lateral movements of the nose tip (right). Filled circles and error bars show mean ± SEM. Lightly colored lines correspond to individual data. *$p < 0.05$, **$p < 0.01$, ***$p < 0.001$, ****$p < 0.0001$, Bonferroni's multiple comparison test.

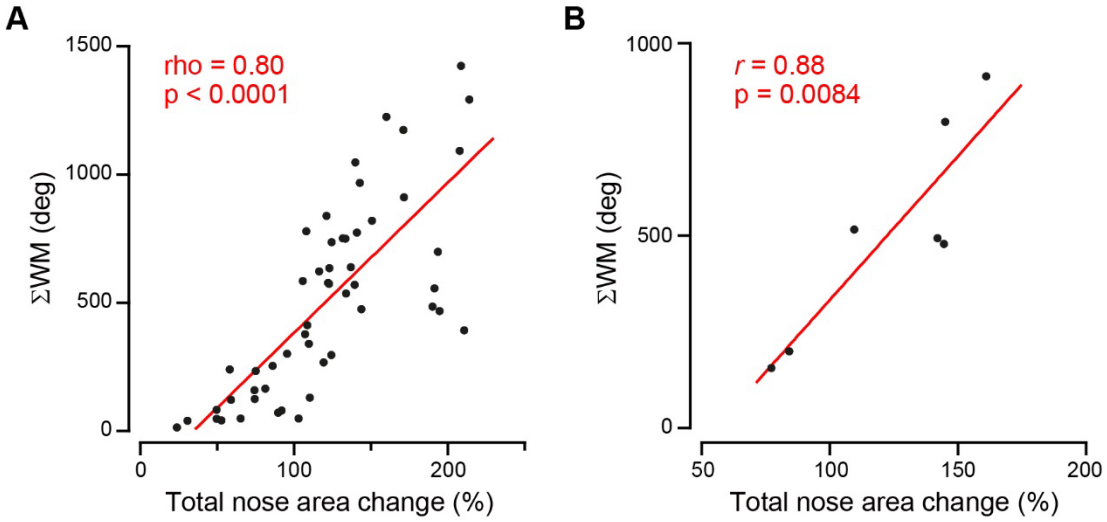

Fig. S3. Correlation between nose and whisker movements induced by oDAS. (**A**) ΣWM as a function of the total change in the nose area for individual oDAS (5 ms x20, 20 Hz) trials (n = 52 trials, from 7 mice). We selected trials without prominent whisking starting 0-1 s before the stimulus onset. Red line: linear regression. (**B**) Same as (A) but for individual mice (n = 7 mice).

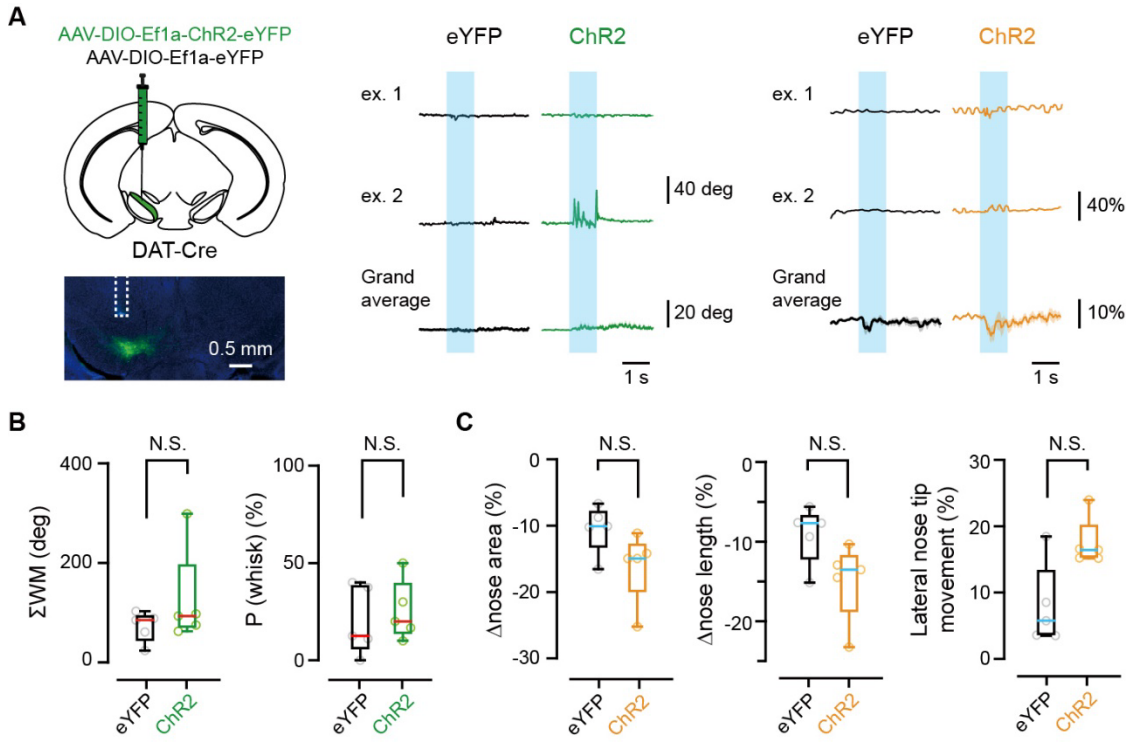

Fig. S4. Optogenetic stimulation of SNc-DA neurons did not elicit orofacial movements. (**A**) Left, schematic for the AAV injection into the SNc (top), and an epifluorescence image of a coronal section containing SNc and the trace of the inserted optical fiber (dashed line) (bottom). Green: ChR2-eYFP, blue: DAPI. Middle and right, example and grand average traces of the whisker position (middle) and the top-view nose area (right) obtained from ChR2- and eYFP-expressing mice (n = 5 for each group). (**B**) ΣWM and the probability of whisking initiation upon optogenetic stimulation of SNc-DA neurons in ChR2- and eYFP-expressing mice. (**C**) Same as (B) but for the parameters of nose movement. Medians of the box plots are shown in red (B) or cyan (C). N.S.: not significant, unpaired *t* test (P(whisk) in B and Δnose area and Δnose length in C) or Mann-Whitney *U* test (ΣWM in B and lateral nose tip movement in C).

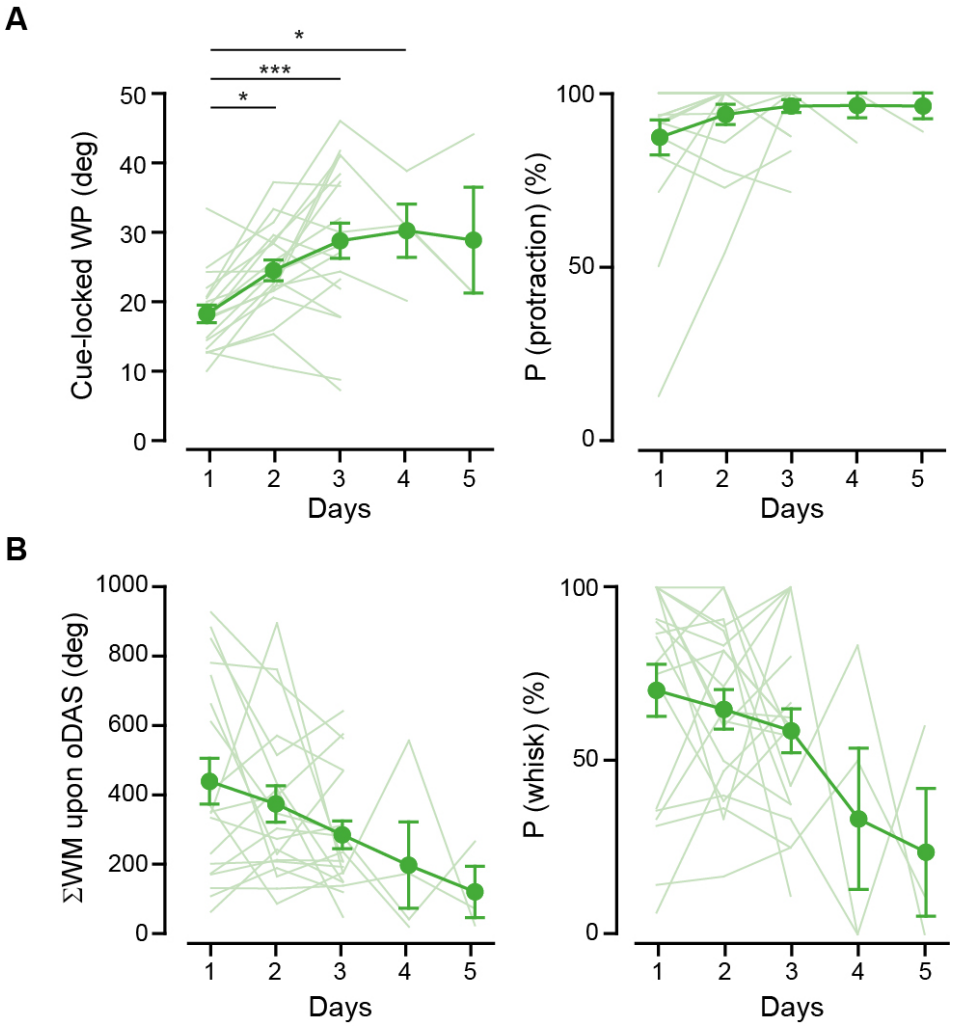

Fig. S5. Additional analyses of whisker movements during the stimulus-oDAS association task. (**A**) Amplitude (left) and probability (right) of cue-locked whisker protraction (WP) of DAT-ChR2 mice on day 1–5 during the sound-oDAS pairing conditioning (day 1–3, n = 19 mice; day 4, n = 4 mice; day 5, n = 3 mice). We performed pharmacological experiments on day 3–5 and data with saline injection (Fig. 5 and fig. S8) or before muscimol/Ringer injection (Fig. 6) were plotted. We did not include data during wM1 recordings (Fig. 7) nor the data from the mice used only for 2 days without pharmacological experiments. (**B**) Total whisker movements (ΣWM, left) and the probability of whisking (right) of the same mice in (A) during oDAS in the sound-oDAS pairing conditioning. Filled circles and error bars show mean ± SEM. Lightly colored lines correspond to individual data. *$p < 0.05$, ***$p < 0.001$, Kruskal-Wallis test followed by Dunn's multiple comparison test, vs. day 1.

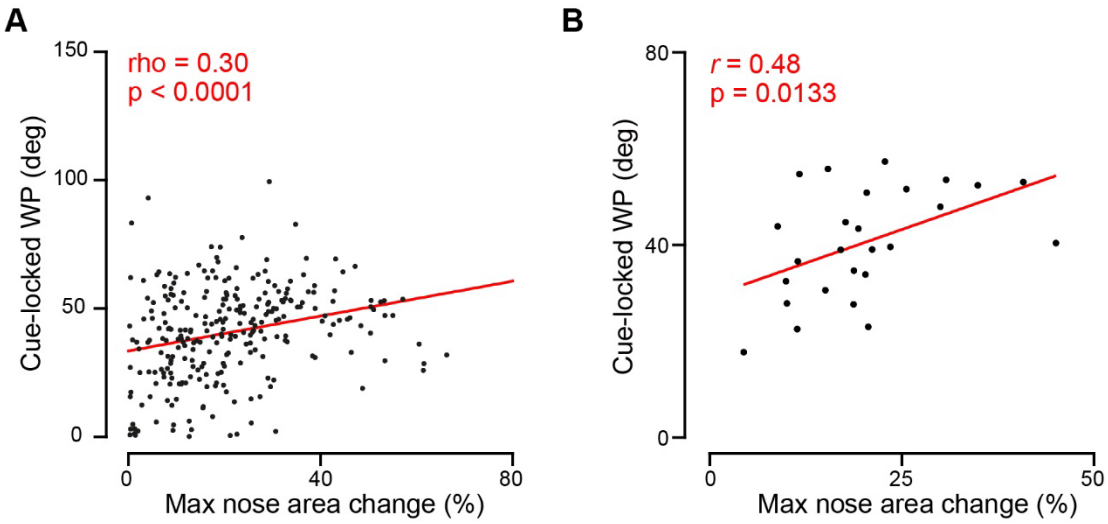

Fig. S6. Correlation between nose and whisker movements at the cue onset of sound-oDAS association. (**A**) The amplitude of cue-locked whisker protraction (WP) as a function of that of cue-locked nose area change for individual trials at day 2 (n = 272 trials, from 26 mice). We selected trials without prominent whisking starting 0-1 s before the stimulus onset. Red line: linear regression. (**B**) Same as (A) but for individual mice (n = 26 mice).

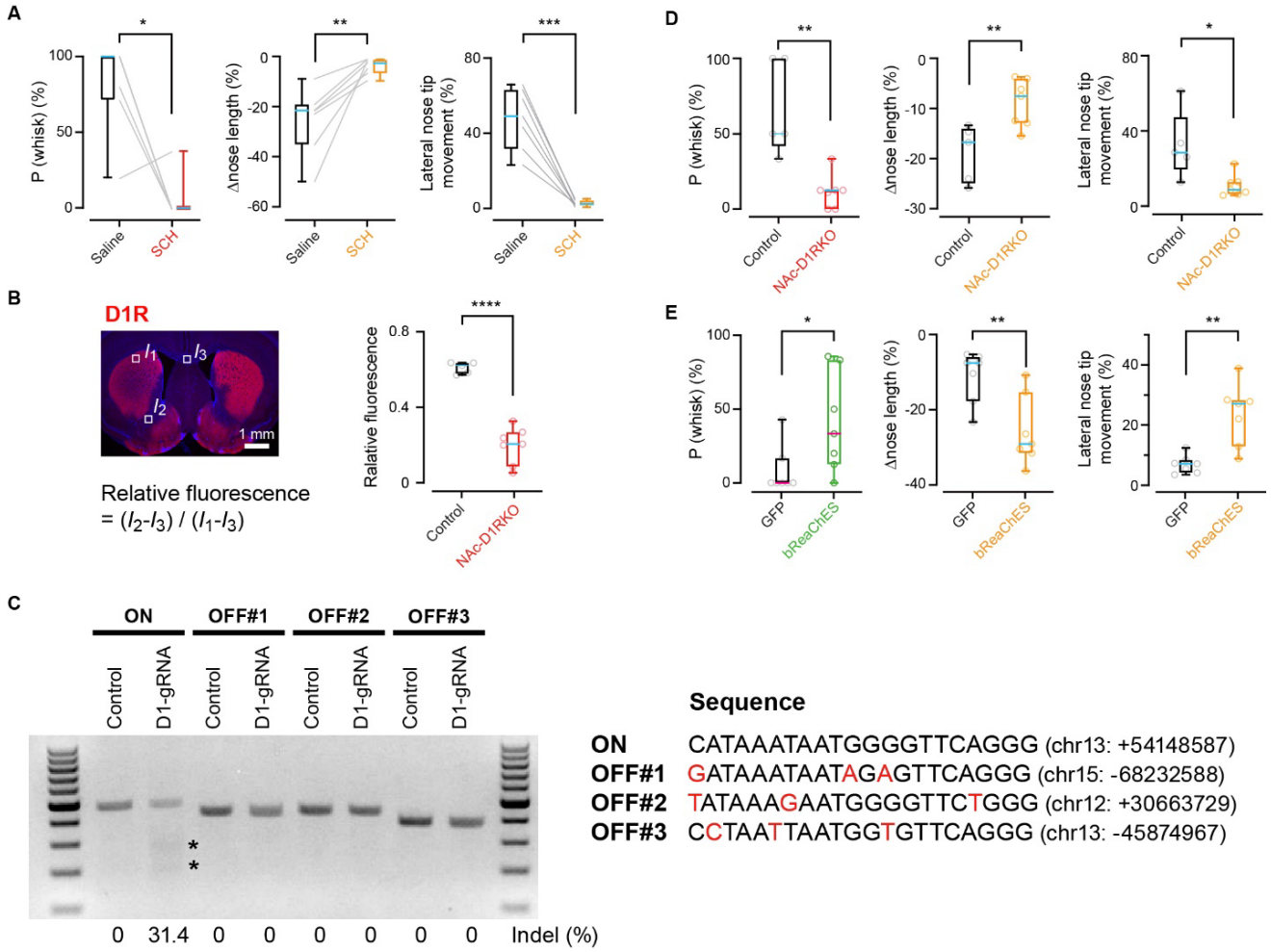

Fig. S7. Additional analyses of perturbational experiments for oDAS-induced orofacial movements. (**A**) Left, data for each mouse (thin lines) and box plots for the parameters of whisker or nose movements in trials after IP injection of SCH23390 (red or orange) and saline (black) during oDAS (n = 7 mice). (**B**) Left, schematic for the fluorescence analysis. Average fluorescent signal intensity (FI) at the region of interest (outlined square) was measured. I_1: FI at the dorsal striatum, I_2: FI at the NAc, I_3: FI at the white matter around the midline. Right, comparison of D1R immunoreactivity at the NAc between mice injected with AAV-gRNA (NAc-D1RKO, n = 7 mice) and AAV-Control (Control, n = 5 mice). (**C**) Surveyor nuclease cleavage assay. The saCas9-*Drd1a*-gRNA (D1gRNA) showed the capacity of cleaving ON-target (ON) *Drd1a* sequence but not the potential OFF-target (OFF) sites with three mismatches (red letters). *: cleavage bands, Control: saCas9 with empty gRNA, chr: chromosome. (**D**) Same as (A) but for data from NAc-D1R-KO (red or orange) and control (black) mice (control: n = 5 mice; NAc-D1R-KO: n = 7 mice). (**E**) Same as (A) but for data from bReaChES- (green or orange) and GFP- (black) expressing mice (n = 7 mice for each). Medians of the box plots

are shown in magenta in (E, left) or in cyan in (A), (D), and (E, middle and right). Open circles and lightly colored lines correspond to individual data. *$p < 0.05$, ** $p < 0.01$, ***$p < 0.001$, paired *t* test (nose length and lateral nose tip movement in A), Wilcoxon singned rank test (P(whisk) in A) or unpaired *t* test (B, D and E).

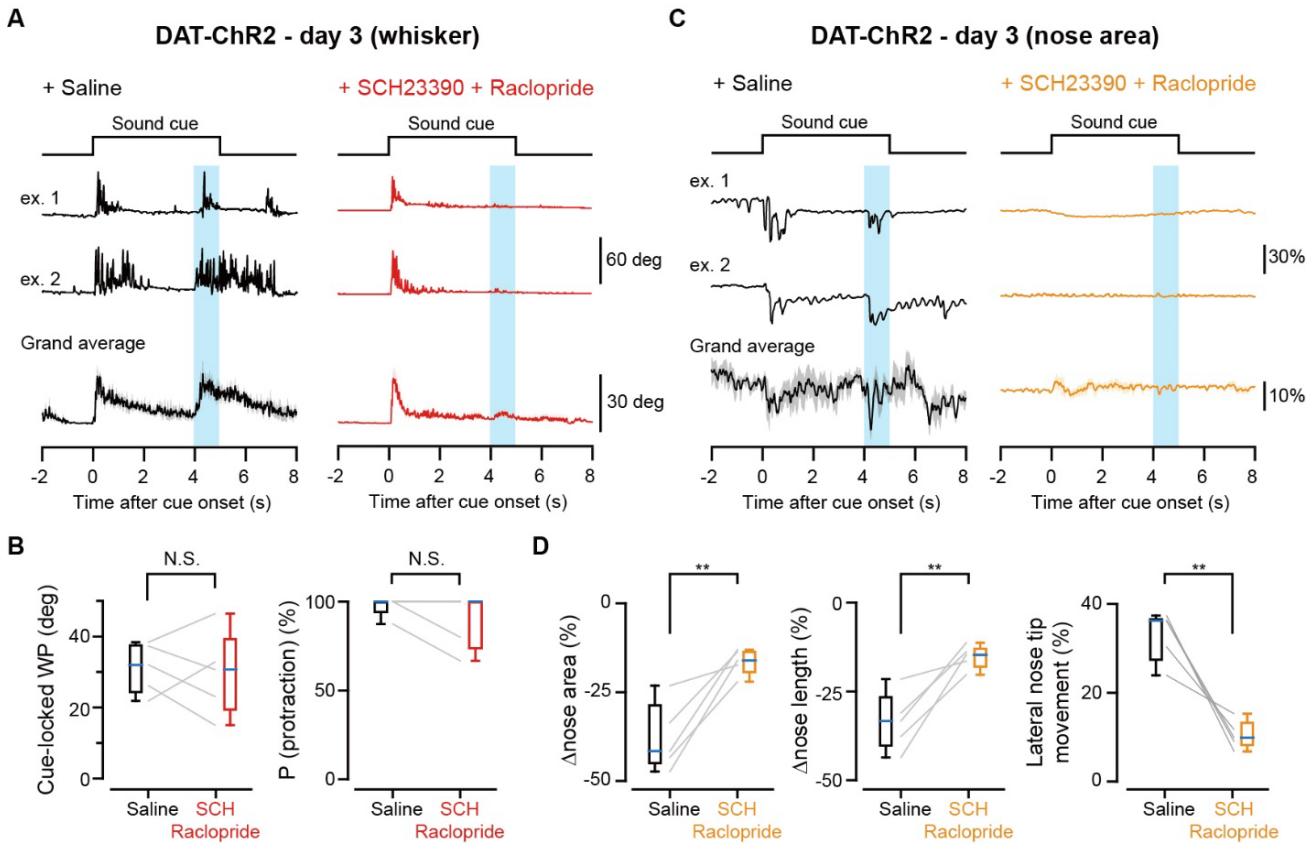

Fig. S8. Orofacial movements upon sound-oDAS pairing under blockade of D1Rs and D2Rs. (**A**) Example and grand average traces of the whisker position in trials with D1R- and D2R-antagonists- (red) or saline- (black) injection in DAT-ChR2 mice during sound-oDAS pairing experiments on day 3 (n = 5 mice). (**B**) The amplitude of cue-locked whisker protraction (WP, left) and protraction probability (right) upon sound cue presentation. (**C**) Same as (A) but for traces of the top-view nose area. (**D**) Same as (B) but for the parameters of nose movement. Medians of the box plots are shown in cyan. Thin lines correspond to individual data. N.S.: not significant, paired *t* test (cue-locked WP in B and D) or Wilcoxon singed rank test (P(protraction) in B).

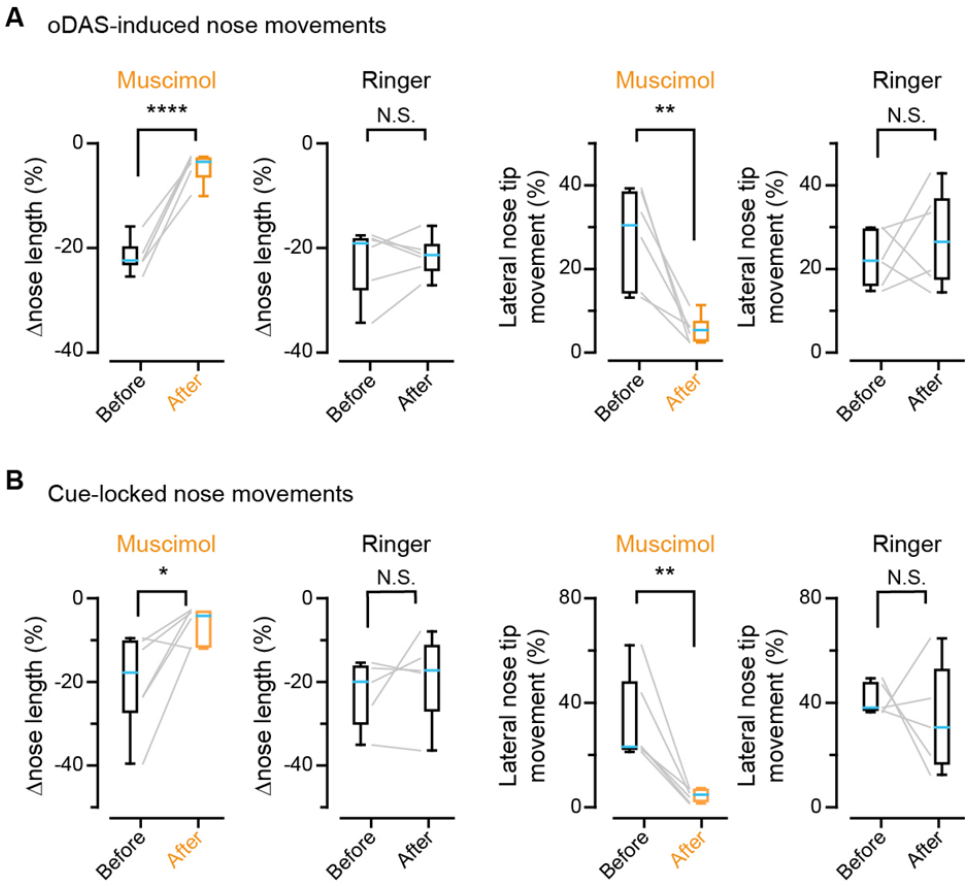

Fig. S9. Additional analyses of orofacial movements upon wM1 inhibition. (**A**) Data for each mouse (thin lines) and box plots for the changes in nose length and the changes in lateral movements of the nose tip in trials before (black) and after (orange) injection of muscimol or Ringer's solution during oDAS (n = 6 mice for each). (**B**) Same as (A) but data at the cue onset during sound-oDAS pairing conditioning on day 3–5 (muscimol, n = 6 mice; Ringer, n = 5 mice). Medians of the box plots are shown in cyan. *p < 0.05, **p < 0.01, ****p < 0.0001, N.S., not significant, paired *t* test (Δnose length for Muscimol and lateral nose tip movement for Muscimol and Ringer in A and Δnose length for Muscimol and Ringer and lateral nose tip movement for Ringer in B) or Wilcoxon singed rank test (Δnose length for Ringer in A and lateral nose tip movement for Musimol in B).

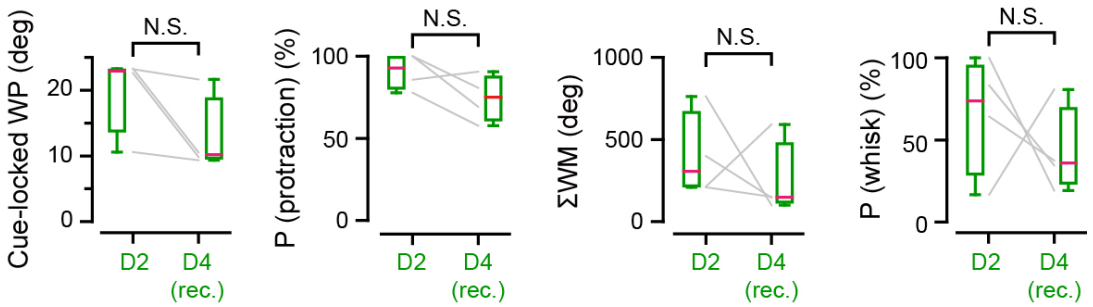

Fig. S10. Reward-related orofacial movements of the mice used for wM1 recordings. Quantifications of the amplitude (most left) and probability (second left) of the cue-locked whisker protraction (WP) and the magnitude (second right) and probability (most right) of whisker movements during oDAS. Data on day 2 (D2) and day 4 (D4) of the sound-oDAS pairing conditioning (Figure 7) were obtained from the four DAT-ChR2 mice used for electrophysiological recordings (rec.) at D4. Medians of the box plots are shown in red. N.S., not significant, paired *t* test for P (protraction) and P (whisk) or Wilcoxon signed rank test for cue-locked WP and ΣWM.

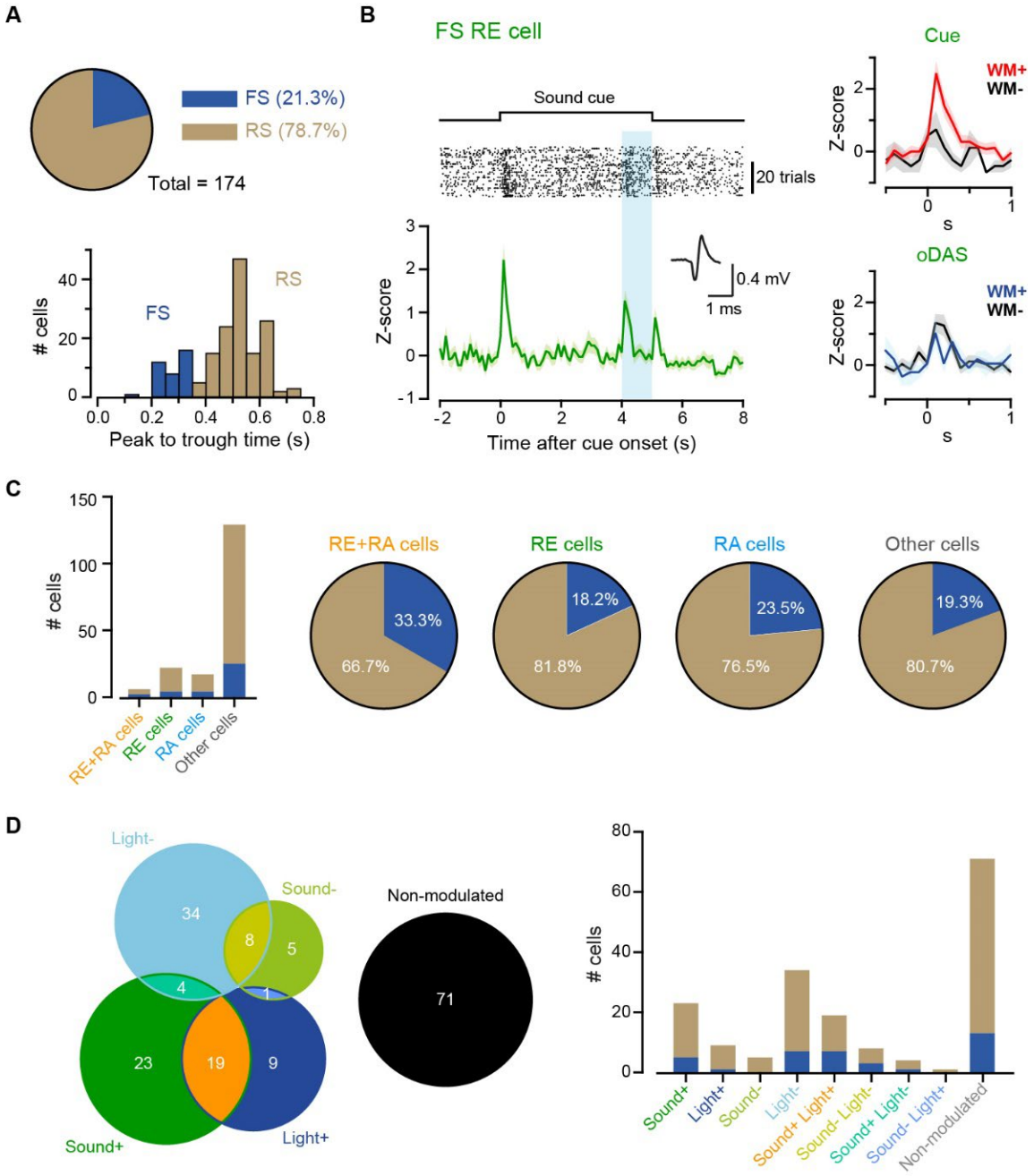

Fig. S11. Additional analyses of neuronal activities in wM1 during the sound-oDAS pairing experiment. (**A**) Top, fraction of fast-spiking (FS, dark blue) and regulate-spiking (RS, copper) cells among recorded units, defined by their peak to trough time of the spike waveform. Bottom, distribution of peak to trough time of recorded units. (**B**) Left, example raster plot (top) and corresponding Z-scored PSTH (bottom) obtained from a representative FS RE cell. The averaged action potential waveform is shown in the inset. Right, Z-scored PSTH of the same cell at around the cue onset (top) and upon oDAS (bottom), comparing data with or without whisker protraction (WP) at the cue onset

or whisker movement (WM) during oDAS. (**C**) Fraction of FS (dark blue) and RS (copper) neurons among recorded units in the cell categories defined by the correlation with reward-related orofacial movements. (**D**) Left, among 174 units in wM1 we studied, 103 units (59.2 %) significantly increased (+) or decreased (-) their firing rate at the cue onset (Sound+ or Sound-) and/or during oDAS (Light+ or Light-). Right, fraction of FS (dark blue) and RS (copper) neurons in different cell categories defined by their responsivity (left).